STIFFNESS REQUIREMENTS OF SHEAR DIAPHRAGMS USED TO BRACE STEEL I-BEAMS

A Thesis Submitted to the
Graduate School of Engineering and Sciences of
İzmir Institute of Technology
in Partial Fulfillment of the Requirements for the Degree of

MASTER OF SCIENCE

in Civil Engineering

by
Andaç AKBABA

July 2017
İZMİR

We approve the thesis of **Andaç AKBABA**

Examining Committee Members:

Assist. Prof. Dr. Carmen Amaddeo
Department of Civil Engineering, Izmir University of Economics

Assoc. Prof. Dr. Cemalettin DÖNMEZ
Department of Civil Engineering, İzmir Institute of Technology

Assist. Prof. Dr. Selçuk SAATCI
Department of Civil Engineering, İzmir Institute of Technology

11 July 2017

Assoc. Prof. Dr. Cemalettin DÖNMEZ
Supervisor,
Department of Civil Engineering,
İzmir Institute of Technology

Assoc. Prof. Dr. Oğuz Özgür EĞİLMEZ
Co-Supervisor,
Department of Civil Engineering
Izmir University of Economics

Prof. Dr. Gökmen TAYFUR
Head of the Department of Civil Engineering

Prof. Dr. Aysun SOFUOĞLU
Dean of the Graduate School of
Engineering and Sciences

ACKNOWLEDGMENTS

I would like to express my deepest gratitude to Assoc. Prof. Dr. Özgür Eğilmez, for his excellent guidance, caring, patience. I would also like to thank Assoc. Prof. Dr. Cemalettin Dönmez, who encouraged me for completing my thesis, supported me with his guidance and patiently corrected my writing.

I would like to thank Mustafa Vardaroğlu, who as a great friend and colleague, was always willing to help and spare his time for me. I also would like to thank my friends, Alper Çankaya, Gülfer Akgün and Mustafa Karaman for their friendship and sharing their experiences on writing thesis and all my colleagues at Department of Civil Engineering Laboratory for their friendship and support.

I would also like to thank my parents. They always supported me and encouraging me with their best wishes.

ABSTRACT

STIFFNESS REQUIREMENTS OF SHEAR DIAPHRAGMS USED TO BRACE STEEL I-BEAMS

The buckling capacity of steel I-beams can be increased by providing lateral bracing along the length of the beams by either cross-frames or diaphragms. Metal sheeting that is often used in steel building and bridge constructions to support the fresh concrete, acts like a shear diaphragm and provides continuous bracing to steel beams. In building industry, metal deck forms are considered as a lateral support to the beams. However, due to their flexible connection detail between the girder and shear diaphragm, metal deck forms are not considered as a brace source for bridge construction industry. But with the recent studies, by improvements of the flexible connection details, metal decking can be used as a bracing system.

An adequate bracing system must possess sufficient stiffness and strength. A computational study was conducted to investigate stiffness requirements of shear diaphragms used to brace stocky and slender steel I-beams. Both doubly and singly symmetric sections were studied. The computational study consists of eigenvalue buckling analyses on perfectly straight twin-girder system braced by shear diaphragms and large deformation analyses with imperfect girders with different configurations of girder sections and spans. A three dimensional computer programme was utilized to perform analytical studies. Analytical model is verified by a full-scale twin-girder system laboratory test that is carried out on a previous study. Stiffness requirements have been proposed for shear diaphragms used to brace stocky and slender steel I-beams.

ÖZET

NARİN ÇELİK KİRİŞLERE STABİLİTE DESTEĞİ SAĞLAYAN KAYMA DİYAFRAMLARININ RİJİTLİK GEREKLİLİKLERİ

Çelik I-kirişlerin burkulma kapasitesi, noktasal veya sürekli destek elemanları kullanılarak artırılmaktadır. Yapım aşamasında taze betonu taşımak için kiriş uzunluğunca kullanılan trapez sac kalıplar, bir kayma diyaframı gibi davranırlar ve çelik kirişlere sürekli destek sağlarlar. Çelik yapı endüstrisinde, sac kalıplar kirişlere yatay destek elemanı olarak değerlendirilirler. Fakat sac kalıplar, kiriş ve kalıp arasındaki bağlantı detayının esnekliğine bağlı olarak, çelik köprü endüstrisinde bir destek elemanı olarak değerlendirilmemektedir. Ama son zamanlardaki çalışmalar, bağlantı detaylarındaki iyileştirilmeler ile sac kalıpların destek elemanı olarak kullanılabileceğini göstermiştir.

Bir destek elemanının görevini yerine getirebilmesi için yeterli rijitliğe ve dayanıma sahip olması gerekmektedir. Narin gövdeli çelik kirişleri destekleyen kayma diyaframlarının rijitlik gerekliliklerini araştırmak için sayısal bir çalışma yapılmıştır. Çift ve tek simetri eksenli kesitler incelenmiştir. Analiz çalışmaları mevcut yamukluğu olmayan kiriş ve kayma diyaframlarından oluşan sistemin öz-değer burkulma analizlerini ve mevcut kusuru bulunan kirişlerden oluşan kayma diyaframlarının büyük deformasyonlar teorisine göre analizlerinden oluşmaktadır. Analizleri yürütmek için üç boyutlu sonlu elemanlar programından yararlanılmıştır. Analitik model daha önceki çalışmalarda kullanılan tam ölçekli bir test modeline ait analiz sonuçlarıyla karşılaştırılmış ve doğrulanmıştır. Kiriş orta açıklığında noktasal destek elemanı bulunduran kirişler de analiz edilmiştir. Narin gövdeli çelik I-kirişleri destekleyen kayma diyaframları için minimum rijitlilik gereklilikleri önerilmiştir.

TABLE OF CONTENTS

LIST OF FIGURES viii

LIST OF TABLES x

LIST OF SYMBOLS xi

CHAPTER 1. INTRODUCTION 1
- 1.1. General 1
- 1.2. Structural Advantages of Metal Deck Forming Systems 2
- 1.3. Objective and Scope of the Study 4
- 1.4. Organization of the Study 5

CHAPTER 2. BACKGROUND AND PREVIOUS STUDIES 6
- 2.1. Introduction 6
- 2.2. Lateral Torsional Buckling Behavior of Steel Members 6
  - 2.2.1. Buckling Capacity of Beams Subjected to Constant Moment 7
  - 2.2.2. Effects of Moment Gradient and Load Height on LTB 9
- 2.3. Stability and Bracing Systems 11
  - 2.3.1. Stability 11
  - 2.3.2. Bracing Systems 12
- 2.4. Beam Bracing 14
- 2.5. Shear Diaphragms as Continuous Bracing Systems 15
- 2.6. Influence of Critical Imperfections on Beam Bracing 16
- 2.7. Previous Studies 20

CHAPTER 3. FINITE ELEMENT MODEL 32
- 3.1. Introduction 32
- 3.2. Finite Element Model and the Loading Procedure 33
- 3.3. FEA Model of Steel I-Girders 34
- 3.4. FEA Model of Shear Diaphragm 38
- 3.5. FEA Model of Fasteners 39

3.6. The FEA Model of Shear Frame 42
3.7. Verification of the FEA Model 44

CHAPTER 4. OVERVIEW OF STUDY 46
4.1. Introduction 46
4.2. Analysis Parameters 46
4.3. Procedures of the Numerical Study 51

CHAPTER 5. FINITE ELEMENT RESULTS 54
5.1. Introduction 54
5.2. Doubly Symmetric I-Beams with Stocky Webs 54
5.3. Doubly and Singly Symmetric I-Beams with Slender Web 61
5.4. Diaphragm Stiffness Requirements of I-Beams 69

CHAPTER 6. CONCLUSIONS 72
6.1. Summary and Conclusions 72

REFERENCES 75

APPENDIX A. DESIGN EXAMPLE 78

LIST OF FIGURES

Figure **Page**

Figure 2. 1. Lateral Torsional Buckling Behavior and Cross Section Twist 7
Figure 2.2. Tennessee River Bridge on the day of collapse. 12
Figure 2. 3. Types of bracing systems. 13
Figure 2. 4. Restraining forces on a steel I-beam. 14
Figure 2. 5. Diaphragm shear behaviour..... 15
Figure 2. 6.Test setup of a typical shear diaphragm at Cornell University. 16
Figure 2. 7. Effect of brace stiffness on deformations using Winter's model. 17
Figure 2. 8. Effect of cross sectional imperfection on brace moments..... 18
Figure 2. 9. Critical shape of imperfection of the cross section. 19
Figure 2. 10. Brace moments versus imperfection magnitude. 19
Figure 2. 11. Sections considered in the study of Helwig and Frank (1999)..... 23
Figure 2. 12. Definition of parameter "e"..... 24
Figure 2. 13. Truss panel model 28
Figure 2. 14. Brace moment and shear on corrugated sheet. 30
Figure 3. 1. Twin girder and metal deck diaphragm system..... 33
Figure 3. 2. SHELL93 Element in ANSYS library. 34
Figure 3. 3. ANSYS FE Model of the girders and beams. 36
Figure 3. 4. The shape and magnitude of imperfections used in the study..... 37
Figure 3. 5. Plan view of imperfections..... 37
Figure 3. 6. Analytical model of twin girder system based on Davies and Bryan. 38
Figure 3. 7. Finite element analytical model of a metal deck..... 39
Figure 3. 8. LINK8 geometry and stress output. 40
Figure 3. 9. FE model of the fastener based on Davies and Bryan..... 40
Figure 3. 10. Transverse diaphragm at the supports..... 41
Figure 3. 11. FE model of shear frame used to measure shear parameters. 43
Figure 3. 12. Comparison of FEM and laboratory test results..... 45
Figure 4. 1. Doubly Symmetric Sections analyzed in the study..... 48
Figure 4. 2. Singly Symmetric Sections analyzed in the study..... 48
Figure 4. 3. General geometry of steel I-beams and girders..... 49
Figure 4. 4. Shear frame model used to determine the shear stiffness of decks..... 53

Figure 5. 1. Normalized applied moment versus normalized mid span twist ratios of Stocky#1 and Stocky#2 beams with an L/d ratio of 30. 55
Figure 5. 2. Brace forces that develop in a single deck sheet. 57
Figure 5. 3. Resultant end fastener brace forces of Stocky#1 and 58
Figure 5. 4. Sidelap fastener forces along the beam for Stocky#1 and Stocky#2 60
Figure 5. 5. Normalized applied moment versus maximum edge fastener forces for Slender 100#1,SS-100#39, #29, #19 beams with an L/d ratio of 15 68
Figure 5. 6. Normalized applied moment versus maximum side lap fastener forces (per fastener) for Slender 100#1,SS-100#39, #29, #19 beams with an L/d of 15.... 69

LIST OF TABLES

Table **Page**

Table 2. 1. “m” values 28

Table 3. 1. Material Properties of ASTM A992-Grade 345 Mpa Steel. 34

Table 4. 1. Sections to be analyzed in the study. 49

Table 4. 2. Slenderness and aspect ratios of webs and flanges. 50

Table 5. 1 Normalized mid-span twist ratios of Stocky beams. 56

Table 5. 2. Normalized brace forces of stocky beams 57

Table 5. 3. Normalized mid-span twist ratios of doubly symmetric slender I-beams. ... 62

Table 5. 4. Normalized brace forces of doubly symmetric slender I-beams. 63

Table 5. 5. Normalized mid-span twist ratios of singly symmetric slender I-beams. 64

Table 5. 6. Normalized brace forces of singly symmetric slender I-beams. 65

LIST OF SYMBOLS

L_b = Unbraced length of the beam (distance between points of full bracing)

E = Young's modulus

I_y = The moment of inertia of the weak axis

J = The St. Venant's torsional constant

G = The shear modulus

G' = Effective shear modulus of the diaphragm

C_w = The warping constant of the beam

d = The distance between the centroids of the flanges

ρ = The ratio of the moment of inertia of the compression flange about the axis through the web to weak axis moment of inertia of the section.

I_x = The moment of inertia of the strong axis

y_0 = The distance between shear center and the centroid of the section

M_{cr} = The elastic torsional buckling capacity

M_u = Maximum design moment of a diaphragm-braced beam;

M_{max} = The maximum bending moment of unbraced part

M_a = The moment at the quarter point of unbraced part

M_b = The moment at the midpoint of unbraced part

M_c = The moment at the three quarter point of unbraced part

C_b = Factor for moment gradient

C_b^* = Moment gradient factor that considers load height effects

h = Depth of the girder

y = The distance between mid-point and the point of applied load

B = Parameter that consists of the warping stiffness and the effects of the type of loading.

P_{cr} = The elastic critical buckling load

P_e = Weak axis Euler buckling load

EI_y = Weak axis bending rigidity

EC_w = Warping rigidity

GJ = Torsional rigidity

e = The distance between the center of gravity of the beam and the plane of the diaphragm

n = A constant for different end support conditions. (1 for simply supported end and 2 for fixed end.)

M_g = Buckling capacity of the girder alone

Q = Shear rigidity of the shear diaphragm

g = Load height factor

θ_0 = Initial twist in radians

s_d = Tributary width of a diaphragm bracing a single beam

n_g = Number of girders in the system

s = Spacing of the girders

M_{br}' = Warping restraining moment per unit length along the longitudinal axis of the beam

F_V = Component of brace force parallel to beam longitudinal axis

F_M = Component of brace force perpendicular to beam longitudinal axis

F_R = The resultant force in fasteners

V_{br} = Shear force in truss panel

n_e = Number of edge fasteners per panel

w_d = width of the shear diaphragm

CHAPTER 1

INTRODUCTION

1.1. General

The cold formed light gauge steel sheets has numerous ways of applications in construction industry such as siding, roof cladding or floor decks. In addition to its use as cover sheets, it could be used as permanent formworks to meet the aesthetic and functional needs of the structures.

Permanent metal deck formworks are cold formed corrugated steel sheets that are coated by hot-dipped galvanization process. The shape of the ribs and the material properties determine the strength and stiffness of the metal deck. Geometry of the ribs changes based on the span and the load level of the metal deck forms. The shipping conditions limit the deck widths to 40 inches. Standard deck widths varies based on the application needs and common sizes are 12, 18, 24, 30 and 36 inches.

One of the common usage of metal decking forms is as composite floor decks. Metals decks needed to serve for some significant tasks in such an application. First task is to provide a working platform for workers. Other tasks are serving as a formwork for concrete slab, stabilization of the frame against lateral torsional buckling and acting as part of the reinforcement of the concrete slab. While floor decks are composite members, roof decking forms are not designed to act together with other structural elements such as steel members and the concrete slab. Its sole purpose is to transfer the lateral and vertical loads to the frames. In comparison with floor decks, rib openings of the roof decking forms are generally shallower to provide just the right room for the thermal insulation boards.

Utilizing metal decks as formwork in structures provides many advantages to the contractor. Erection of metal decking is fast and easy. The provided working platform provides a safer working environment for the workers. Also, due to the efficient material use, economical solutions are achieved as well.

1.2. Structural Advantages of Metal Deck Forming Systems

As it is mentioned above, in addition to its non-structural advantages, metal deck forms have structural purposes. It could be used for the purpose of structural stability of members, such as beams, columns, and purlins which they are fastened to. In the steel building and bridge constructions, permanent metal decks behave like a shear diaphragm and support the top flange of beams or girders by restraining the warping deformations and providing lateral bracing. The beam bracing systems could be classified as lateral or torsional bracing. Shear diaphragm bracing could be included in the lateral bracing category. The forming systems used in the bridge and building industry differ in terms of both geometry and connection details. In Figure 1.1 depicts a typical deck form used in bridge applications.

Figure 1.1. A typical deck form used for bridge applications.

In the building industry, the metal deck forms are directly attached to the top flanges of the beams and provides a continuous bracing against LTB. But due to the eccentric connections demonstrated in Figure 1.2, current AASHTO LRFD specifications (2010) do not permit the metal deck forms to be used as a brace element for the bridge I-girders. However, recent studies have showed that metal deck forms could increase the lateral torsional buckling capacity of girders significantly through the modification of the connection details in a relatively simple way as showed in Figure 1.3. (Egilmez et al. 2007 and 2012).

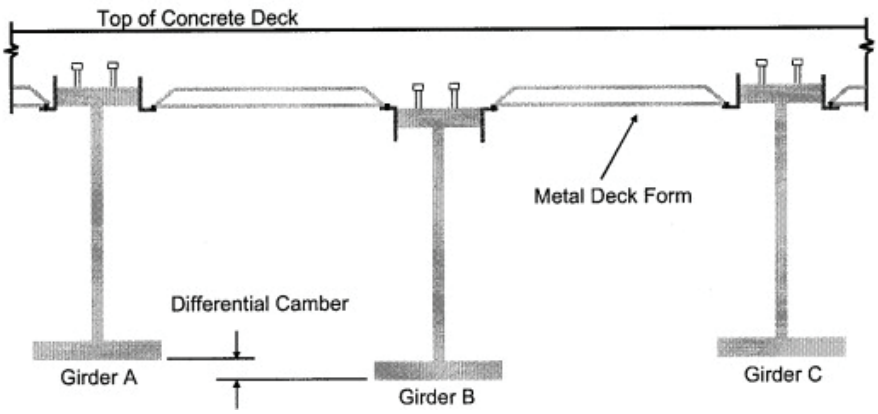

Figure 1.2. Decking detail for bridge applications
(Source : Egilmez, 2005).

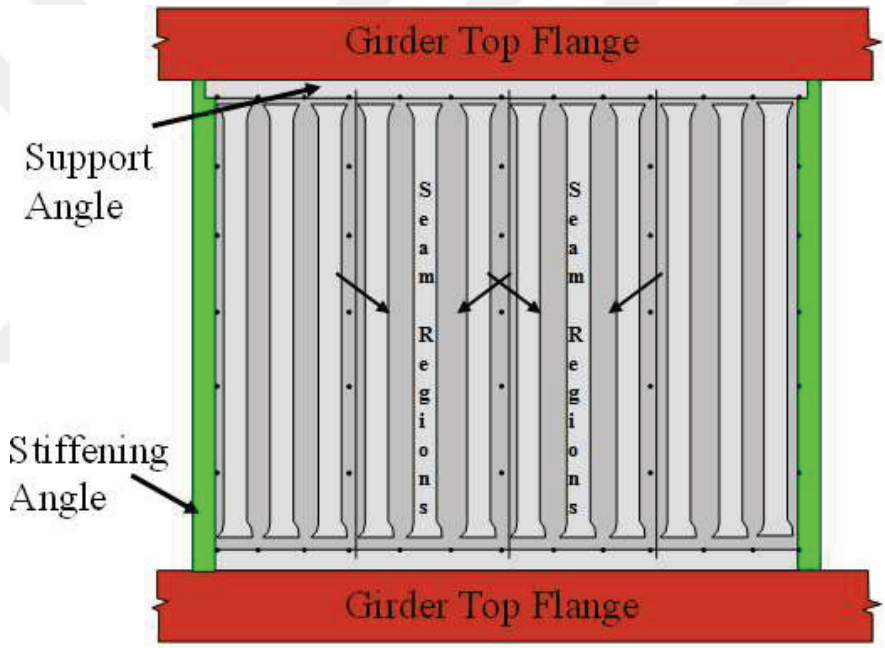

Figure 1.3. Modified deck connection studied by Egilmez et al. 2005.

The main philosophy of the stability bracing design is to ensure that the braced member could carry the design loads while restraining the deformations. To achieve such a purpose, the stiffness and the strength requirements of the bracing system must be satisfied (Winter, 1960). Shear diaphragms have a substantial amount of in-plane-stiffness and strength. The role of shear diaphragms in bracing have been examined in the past (Errera and Apparao, 1976, Nethercot and Trahair, 1975, Helwig and Frank, 1999). In these efforts, the main objective was to study the lateral torsional buckling capacity of

the beams that are supported by diaphragms. The most notable work that explains stiffness and strength requirements of shear diaphragms was performed by Helwig and Yura (2008a and 2008b). In these studies, stocky beams were utilized to determine the stiffness and strength requirements of shear diaphragms without considering the effects of side-lap fasteners.

1.3. Objective and Scope of the Study

The aim of the study presented in this thesis is to improve the understanding of the bracing role of shear diaphragms and to enhance bracing demands for stocky and slender steel I-beams. Analyses were conducted to recommend a specific stiffness value in terms of the ideal stiffness value. Previous studies (Luttrell 1981, Davies and Bryans, 1982) on stiffness and strength requirements of shear diaphragms revealed that the shear strength of a diaphragm is usually controlled by either the shear strength of the connection between the panel sheets and the structural member along the edges or the shear strength at the connections between panel sheets on side-lap zones. Thus, both edge and side-lap fasteners must be considered to develop strength requirements of the shear diaphragms. To achieve this, a simple finite element (FEA) model, that was developed by Davies and Bryan (1982) to examine fastener forces, was used. In order to obtain fastener forces directly, edge and side-lap fasteners were created separately. Since the fastener forces are directly proportional to brace stiffness (Winter 1960, Helwig and Yura, 2008a) a specific brace stiffness must be determined to develop strength requirements for shear diaphragms.

Beam sections considered in this study have relatively stocky and slender webs. Web slenderness ratios of the beams were 100 and 160 for the sections. Both doubly and singly symmetric sections were utilized. Beam depth of the sections were 366 and 732 mm for the stocky beams; 1464 and 1830 mm for both doubly and singly symmetric beams. Span-to-depth ratios of 15, 20, 25 and 30 were studied for stocky beams while 10 and 15 were taken for the slender beams. 610 mm width of deck panels were modelled in the study that were connected to top flange of the beams by four edge fasteners and to the adjacent deck by five side lap fasteners. Thickness of the decks were 1.52 mm (16 ga). The level of the applied force was determined by the load that results in 210 MPa of a bending stress on the extreme fiber of the section.

1.4. Organization of the Study

In this chapter a brief information was given about permanent metal deck forms, application fields and contribution of the lateral stability of the beams. Objective and scope of the study was explained subsequently. In the following chapter, previous studies on shear diaphragms to brace the steel I-beams were clarified. Next chapter consists of a description of the finite element model used and its verification. In chapter four, overview of the study is provided. This chapter involves information about the cross sectional properties of beams used and the type of the analyses conducted in the study. Results from the parametrical study along with stiffness requirements are presented in Chapter 5. The final chapter provides a summary and conclusions.

CHAPTER 2

BACKGROUND AND PREVIOUS STUDIES

2.1. Introduction

This chapter consists of brief information about lateral torsional buckling behaviour of beams and bracing systems utilized to resist this mode of failure. For doubly-symmetric and singly-symmetric beam sections, factors affecting the lateral torsional buckling will be examined. Discussion of the fundamentals of the stability theory and the beam bracing will follow. Afterwards, influence of critical imperfections on stability behaviour of beams will be discussed. The discussions on the shear diaphragms and the determination of shear rigidity values used in the analyses will follow. The last section will be about the previous studies conducted about the topic.

2.2. Lateral Torsional Buckling Behavior of Steel Members

Main resistance mechanism of beams and girders to transverse loading is the major axis bending. Yet in I-shaped steel beams or girders, minor axis behaviour could controls the failure mode. Since the major axis stiffness is much larger than the minor axis, the weakness in the minor axis pronounced in the torsional properties of the members. Therefore, member could become become more vulnerable to lateral torsional buckling (LTB). If the member does not have adequate bracing against the LTB, it buckles and loses its stability without reaching the flexural yielding strength in major axis. Compression in the top flange that is caused by flexural moment is the root cause of the LTB.

Lateral torsional buckling is a mode of failure that involves an out of plane displacement of the member and twist of the cross section about the shear centre. Figure 2. 1 demonstrates a typical LTB mode of a beam and twist of cross section.

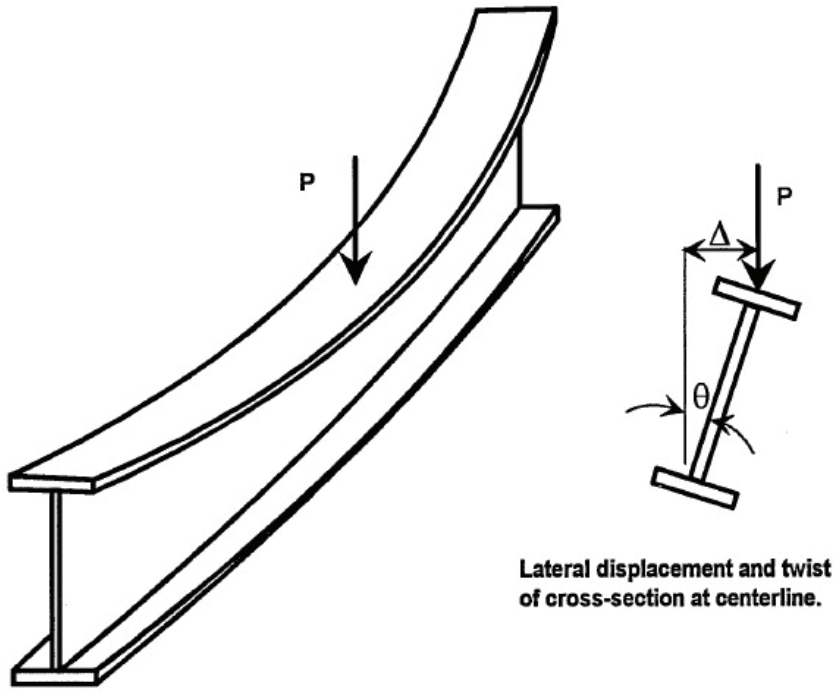

Figure 2. 1. Lateral Torsional Buckling Behavior and Cross Section Twist .
(Source : Guide to Stability Design Criteria for Metal Structures, 2010)

Loading types and height of the load application point have significant roles on determination of the lateral torsional buckling capacity of the girders. The centre of twist, which is defined as the intersection of the axis lines of unbuckled and buckled girders, may lie in different positions through the web. If it is closer to the compression flange, brace effectiveness reduces.

2.2.1. Buckling Capacity of Beams Subjected to Constant Moment

Timoshenko and Gere (1961) derived an equation to calculate the elastic torsional buckling capacity of doubly-symmetric members under constant moment. As boundary conditions, it is assumed that the lateral displacement and the twist of the member is prevented while it is allowed to rotate laterally and free to warp. With these assumptions, the equation below was stated.

$$M_{cr} = \frac{\pi}{L_b}\sqrt{EI_yGJ + (\frac{\pi E}{L_b})^2 I_y C_w} \tag{2.1}$$

Where, L_b is the unbraced length of the beam (distance between points of full bracing), E is Young's modulus, I_y is the moment of inertia of the weak axis, J is the St. Venant's torsional constant, G is the shear modulus and C_w is the warping constant of the beam. The warping constant C_w is calculated by the general equation below. For doubly-symmetric sections, it can be simplified as $C_w = I_y d^2/4$.

$$C_w = I_y d^2 \rho(1-\rho) \tag{2.2}$$

Where d is the distance between the centroids of the flanges, ρ is the ratio of the moment of inertia of the compression flange about the axis through the web to weak axis moment of inertia of the section. The buckling capacity of the beam is obtained by the summation of the St. Venant's torsional resistance and the warping resistance.

In bridge construction, sections of the girders are designed considering the increase of the effective section after casting of the concrete. Due to the composite action after the hardening of concrete, capacity of the member in the compression zone increases considerably. Therefore, it is possible to employ smaller compression flanges at the top. The concrete deck provides a continuous lateral support along the girder as well. Thus, size of the top flanges could decrease further as the lateral torsional buckling is not a critical mode after the development of the composite behaviour. Use of different size flanges resulted singly-symmetric sections. It should be noted that the equation 2.3 is not applicable for singly-symmetric members.

Kitipornchai and Trahir (1980) suggested the equation below to calculate the buckling capacity of the singly-symmetric sections under uniform moment.

$$M_{cr} = \frac{\pi}{L}\sqrt{EI_y}\left(B_1 + \sqrt{1 + \frac{\pi^2 a^2}{L^2} + B_1}\right) \tag{2.3}$$

Where;

$$a = \sqrt{\frac{EC_w}{GJ}} = \sqrt{\left(\frac{E}{GJ}\right)(I_y d^2(\rho(1-\rho)))}$$

$$B_1 = \frac{\pi}{2}\frac{\beta_x}{L}\sqrt{\frac{EI_y}{GJ}}$$

$$\beta_x = \frac{1}{I_x}\int_{dA} y(x^2 + y^2)dA - 2y_0$$

I_x is the moment of inertia of the strong axis and y_0 is the distance between shear center and the centroid of the section.

Due to complexity of the expression, Kitipornchai and Trahir (1980) derived several equations to simplify the solution for singly-symmetric sections, Eq.2.3 express the approximate solution recommended in American Institute of Steel Construction (AISC) Load and Resistance Factor Design (LRFD) Spefication.(AISC-LRFD,2001).

$$M_{cr} = \frac{\pi}{L_b}\sqrt{EI_y GJ}(B_1 + \sqrt{(1 + B_2 + B_1^2)} \tag{2.4}$$

where;

$$B_1 = 2.25(2\rho - 1)(\frac{d}{L_b})\sqrt{\frac{I_y}{J}}$$

$$B_2 = 25(1-\rho)(\frac{I_{yc}}{L_b})(\frac{d}{L_b})^2$$

The variables in the equations were as defined previously.

For singly-symmetric sections, a modified version of Timoshenko's equation for calculating the lateral buckling capacity of doubly-symmetric sections is expressed in the AASHTO Specification as well.

$$M_{cr} = \pi E(\frac{I_{yc}}{L_b})\sqrt{\frac{2G}{E}(\frac{J}{I_{yc}}) + \pi^2\left(\frac{d}{L_b}\right)^2} \tag{2.5}$$

In Eq. 2.5, all the variables are as defined in the equations above except the variable "d". While the variable "d" is defined to be distance between flange centroids in the previous equation, in AASHTO Specification it refers to full girder depth.

2.2.2. Effects of Moment Gradient and Load Height on LTB

Lateral buckling capacity of the doubly-symmetric and singly-symmetric sections under constant moment was expressed in the equations 2.1 to 5. But in real life conditions, beams are typically subjected to transverse loadings. Such a loading result in a moment gradient, which substantially increase the estimated buckling capacity of the members. In transverse loading conditions, moment along the member height varies and the effect of the variation on the buckling capacity is reflected by a modification factor in the previously stated equations. The modification factor, C_b, is defined as a magnifier of the

LTB capacity in transverse loading cases at which the loading is applied at the shear center of the cross section (Galambos 1998).

In order to obtain the moment gradient C_b, The AISC Specification (AISC-LRFD, 2010) suggests Eq. for girders loaded at shear center for doubly symmetric members.

$$C_b = \frac{12.5M_{\max}}{2.5M_{\max} + 3M_A + 4M_B + 3M_C} \tag{2.6}$$

where ;

M_{max} is the maximum bending moment of unbraced part

M_a is the moment at the quarter point of unbraced part

M_b is the moment at the midpoint of unbraced part

M_c is the moment at the three quarter point of unbraced part

For singly-symmetric members, a simple modification is required to Eq.2.6.

$$C_b = R\left[\frac{12.5M_{\max}}{2.5M_{\max} + 3M_A + 4M_B + 3M_C}\right] \leq 3 \tag{2.7}$$

where ;

$R = (0.5+2\rho^2)$ and ρ is as previously defined as ratio of monosymmetry (I_{yc}/I_y).

Since the location of the loading has a significant effect on the twist of the girder, buckling capacity is also effected by the location of the loading. For instance, loading at the top flange reduces the buckling capacity of the girder.

The SSRC Guide (Galambos, 1998) suggests Eq. 2.8 for girders without intermediate discrete bracing.

$$C_b^* = C_b B^{2y/h} \tag{2.8}$$

Where h is depth of the girder, y is the distance between mid-point and the point of applied load and B is a parameter that consists of the warping stiffness and the effects of the type of loading. For mid-span point load and uniformly distributed load cases, B is obtained respectively in the following equations;

$$B = 1 - 0.180W^2 + 0.649W \tag{2.9}$$

$$B = 1 - 0.154W^2 + 0.535W \tag{2.10}$$

$$W = \frac{\pi}{L}\sqrt{\frac{EC_w}{GJ}}$$

Where L is the distance between braces, and all the other parameters are as defined before.

Considering the complexity of the calculation of parameter B, the SSRS Guide (Galambos, 1998) recommends B is taken as 1.4 for typical cases.

Eq.2.8 is valid for doubly symmetric sections. For singly-symmetric sections, by taking B parameter as 1.4, following equation can be used for both doubly and singly symmetric sections conservatively.

$$C_b = R(1.4^{2y/h})\left[\frac{12.5M_{\max}}{2.5M_{\max} + 3M_A + 4M_B + 3M_C}\right] \tag{2.11}$$

2.3. Stability and Bracing Systems

2.3.1. Stability

In applied mechanics history, Swiss mathematician Leonard Euler has a very important role. After the publication of his well-known column formula, there have been serious research and developments in applied mechanics discipline. The formula in Eq. 2.12 determines the elastic critical buckling load of a perfectly straight column that has simple support boundary conditions.

$$P_{cr} = P_e = \frac{\pi^2 EI}{L^2} \tag{2.12}$$

Where, P_e refers to Euler critical buckling load. The other parameters were as defined in the previous captions.

Following Euler's studies, researches on stability behaviour of members have gained momentum.

When a member subjected to a gravitational loads, it is subjected to bending about its major axis. If an I-beam is considered, while top flange shortens under compression bottom flange of elongates in tension. At a critical loading limit, the top flange start to

move to sideway and could not shorten under compression anymore. The web and tension flange of the beam resist that movement up to a certain limit. Due to inadequate lateral supporting of the top flange, the beam loses its lateral stability and could not reach the yielding of the top flange.

In Figure 2.2, Tennessee River Bridge is depicted on the day of its collapse due to LTB caused by lack of bracing. The bridge lost its lateral stability and collapsed during the construction.

Figure 2.2. Tennessee River Bridge on the day of collapse.
(Source:https://failures.wikispaces.com/Tennessee+River+Bridge+Collapse).

2.3.2. Bracing Systems

Figure 2.2 reflects the importance of bracing in stability problems. Bracing systems that increase the stability of the structures can be classified in four categories as illustrated in Figure 2. 3.

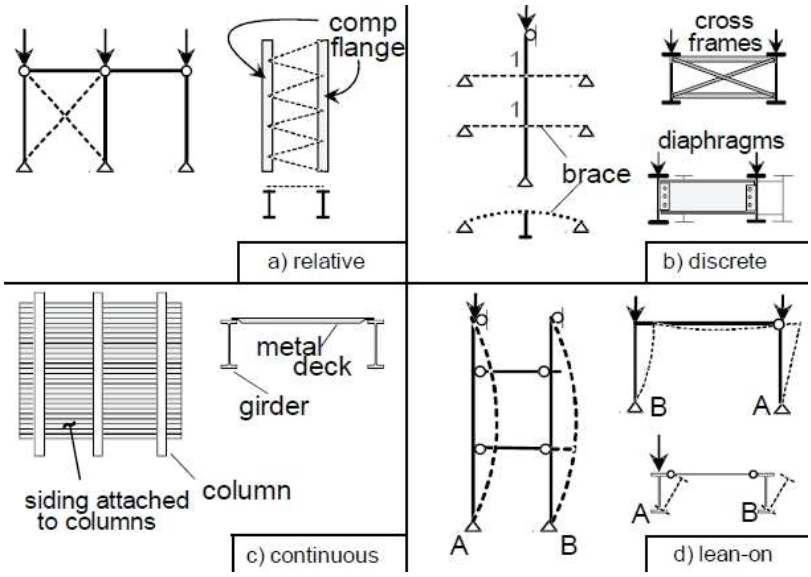

Figure 2. 3. Types of bracing systems.
(Source : Guide to Stability Design Criteria for Metal Structures, 2010)

Truss bracing and diagonal bracing between two structural members are good examples of relative bracing, Figure 2. 3 (a). Bracing members prevent the relative displacement of the points attached to on the structural member.

Discrete bracing, that controls the movement of a single point, is a widely used system as well. As in Figure 2. 3 (b), plate diaphragms and cross frames are in discrete bracing category. Cross frames contributes the stability of the girder since it limits the twist of the girder at a single place.

In Figure 2. 3 (d) lean-on bracing system is depicted. In this concept, leaning members supported by the load carrying system laterally by the provided strut connections.

Another category of the bracing systems, continuous braces restrain the lateral movement of the entire member along its length. Figure 2. 3 (c). Concrete floor deck that provides composite action by shear studs welded on the top flange of the girders and restrains it laterally and torsionally.

2.4. Beam Bracing

Bracing of beams can be outlined in two basic categories as lateral and torsional braces. Relative displacement of top and bottom flanges must be restricted by the braces. (Guide to Stability Design Criteria for Metal Structures, 2010). Lateral braces restrain the movement of the compression flange that are attached to. The reason to attach lateral braces to the top flange is that bracing becomes less effective when it is close to the shear centre. Torsional braces such as diaphragm plates or cross frames prevent the twist of the adjacent girders. A combined way of bracing that keeps the section both laterally and torsionally, explained by Utton and Trahir (1973) and Tong and Chen (1988), is more effective than the individual lateral or torsional brace methods. Metal deck systems that are attached to the compression flange behaves as a shear diaphragm and provides warping restraint to the top flange by limiting cross sectional twist and relative displacements. Figure 2. 4 illustrates the restraining forces on a steel I-girder.

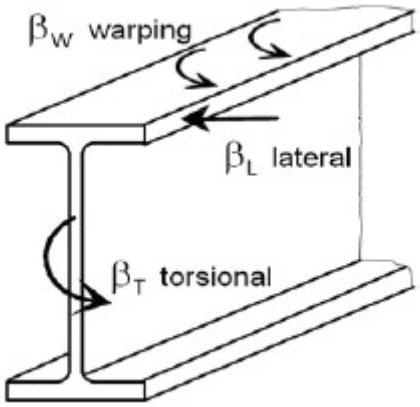

Figure 2. 4. Restraining forces on a steel I-beam.
(Source : Guide to Stability Design Criteria for Metal Structures, 2010)

Helwig and Yura (2008) have stated that in such systems, strength of the diaphragm is limited by fastener capacity.

2.5. Shear Diaphragms as Continuous Bracing Systems

Shear diaphragms which resist to in plane loads are considered to have a membrane-like behavior, (Strength and Behaviour of Light-gage Steel Shear Diaphragms, 1967). With tension field action capability, thin plane sheet and membranes can be defined as the ideal shear diaphragms. Due to their membrane-like behavior and high in-plane rigidities, when permanent metal deck formworks designed properly, it contributes the stability of the girders that they attached to. The most significant property of permanent metal deck forms is shear rigidity, denoted by variable Q has kN/rad as unit. In building industry, it can be used as continuous bracing systems when the ribs attached to top flange perpendicularly. Yet in bridge industry, current AASHTO Specification does not allow permanent metal deck forms to be counted as a bracing member. This ban is due to decrease of the shear rigidity because of differential camber. Figure 2. 5 illustrates the related diaphragm action.

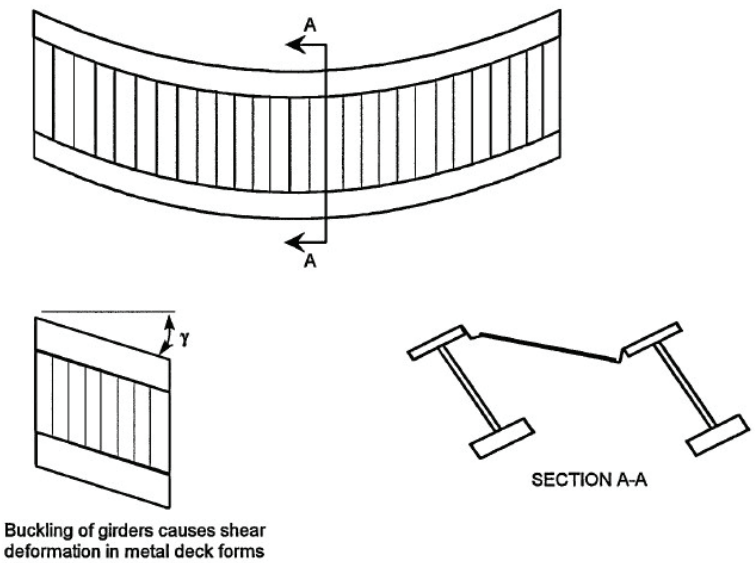

Figure 2. 5. Diaphragm shear behaviour.
(Source : Guide to Stability Design Criteria for Metal Structures, 2010)

Lutrell at. al (1967), carried out a project on behaviour of light-gauge steel diaphragms at Cornell University and published a report. (Strength and Behaviour of Light-Gage Steel Shear Diaphragms, 1967). Various types of diaphragm tests were

reported. Figure 2. 6 portrays a test setup of a typical shear diaphragm utilized at Cornell University. The results of the test, specifically the calculation of shear rigidity values, is discussed in Section 1.7.

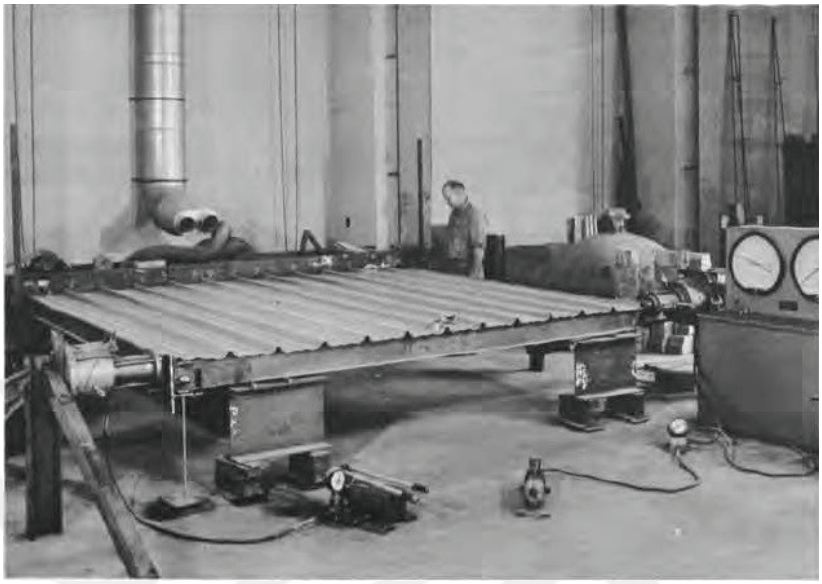

Figure 2. 6.Test setup of a typical shear diaphragm at Cornell University.
(Source : Strength and Behavior of Light-gage Steel Shear Diaphragms)

2.6. Influence of Critical Imperfections on Beam Bracing

Lateral torsional buckling is a critical failure mode that generally controls the design of flexural members. In order to mobilize the capacity of a member, unbraced length must be sufficiently reduced by adding bracing elements to the system. AISC (2001) involves design rules for stability bracing elements. These rules take both stiffness and strength requirements into consideration. While deriving stability-bracing rules, finite element analyses (FEA) could be utilized. Modeling techniques and geometry of the finite element model (FEM) must be properly set to obtain effective results for stiffness and strength requirements. Therefore, boundary conditions and geometrical imperfections should be considered. Initial imperfections of structural members could dictate the bracing behavior of the systems with their effects on brace forces.

Eigen value buckling analyses that are performed by modeling perfectly straight members provide minimum brace stiffness which is called as ideal brace stiffness. In previous studies, Winter (1960) and Yura (2001) showed that the ideal brace stiffness

does not reflect sufficient behavior of the real structures due to geometrical imperfections. Winter (1960) developed a FEM that demonstrated the stiffness requirements and initial imperfection effects. In Figure 2. 7, Winter's column model with a lateral brace at the mid-height and normalized load versus displacement graph are demonstrated. When the ideal stiffness is provided to an imperfect column, it is obvious that it cannot reach the buckling capacity of a perfectly straight member and displacement will be very large. Figure 2. 7 clearly shows that a larger stiffness value than the ideal stiffness could provide the needed behavior and displacements could be controlled. AISC (2001) recommends using two times of the ideal stiffness ($2\beta_i$) to sufficiently control the deformations and reduce the brace forces.

Winter's model focused on flexural buckling of an imperfect column. Buckling mode of such a member involves lateral displacement of the column section. The critical imperfection type of such a member is the translation of the section. For torsional bracing system, the critical imperfection type involves twist of the section. Helwig and Yura (1999) studied torsional behavior of the columns before. Beams elements have different critical imperfection types due to lateral torsional buckling. In LTB, cross section twists in addition to a lateral displacement of the compression flange. Therefore, it is more complicated to select a critical shape for beam elements during buckling.

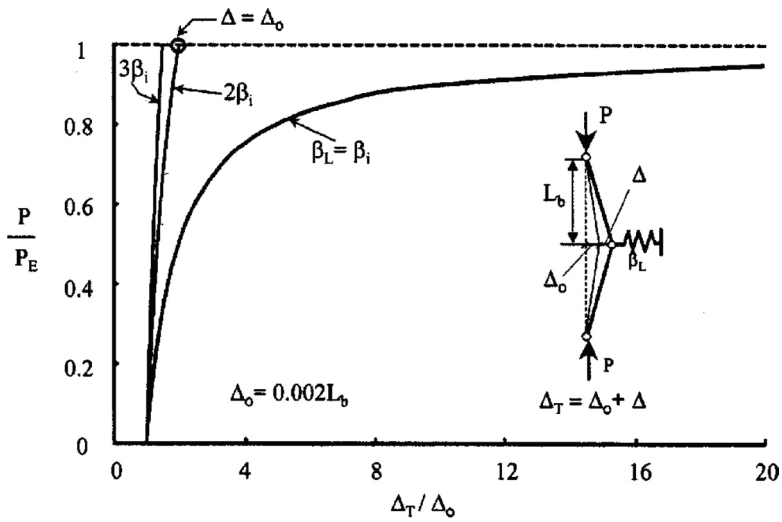

Figure 2. 7. Effect of brace stiffness on deformations using Winter's model.
(Source: Critical Imperfections for Beam Bracing Systems, Wang and Helwig, 2005)

Shape and the magnitude of the imperfections and its distribution along the length are essential factors to be studied. Wang and Helwig (2005) conducted an inclusive research by applying these factors with their (FEM). Their study first focused on obtaining the critical imperfection shape. Then, the distribution of the imperfection along the member was studied. Wang and Helwig (2005) considered a simply supported W14x22 beam to study the cross sectional shape of critical imperfection with a single torsional brace at the mid-span of the beam. Figure 2. 8 graphs a relation between point load at mid-span and torsional brace moment. Each curve represents a different imperfection type. As seen in the figure, Case A is the worst imperfection type for maximizing the brace forces. In Case A, compression flange has a lateral sweep while the tension flange remains straight.

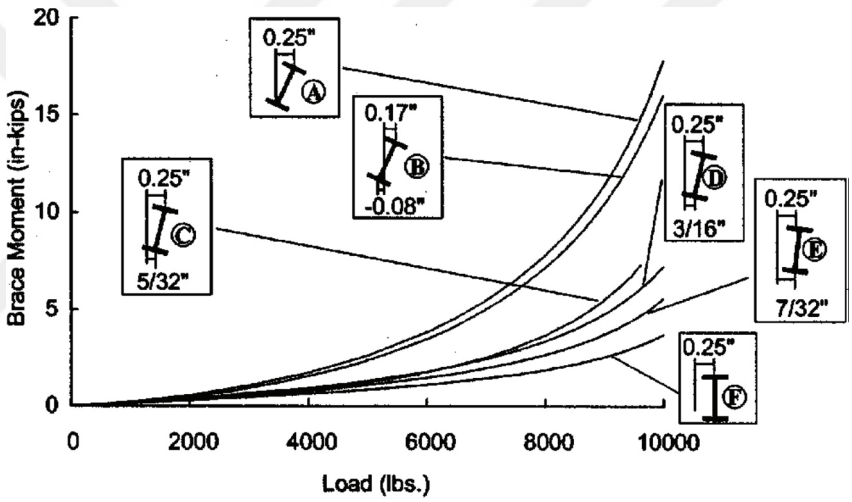

Figure 2. 8. Effect of cross sectional imperfection on brace moments.
(Source: Critical Imperfections for Beam Bracing Systems, Wang and Helwig, 2005)

Results in Figure 2. 8 demonstrates that critical imperfection shape of the cross section is as shown in Figure 2. 9 The magnitude of the imperfection is selected as $L_b/500$ where L_b is the unbraced length. Wang and Helwig (2005) compared the results by taking half and double of the $L_b/500$ magnitude. Normalized brace moments at levels of $M/M_{cr}=1$ versus the magnitudes of lateral sweep of top flange at $L_b/1000$, $L_b/500$ and $L_b/250$ is graphed in Figure 2. 10. These results clarifies that smaller imperfections provides reasonable approach when the brace moments are scaled from the values of assumptions made while deriving general provisions.

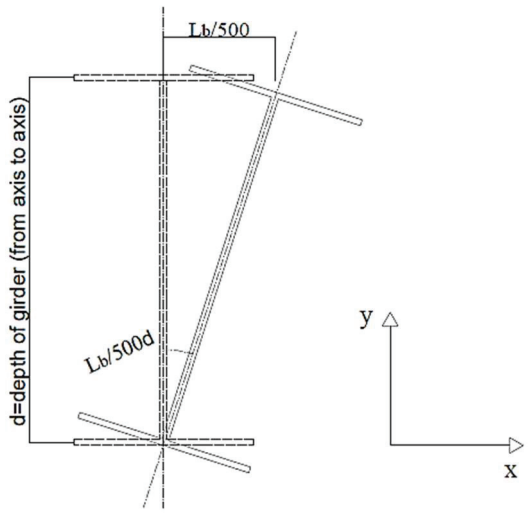

Figure 2. 9. Critical shape of imperfection of the cross section.

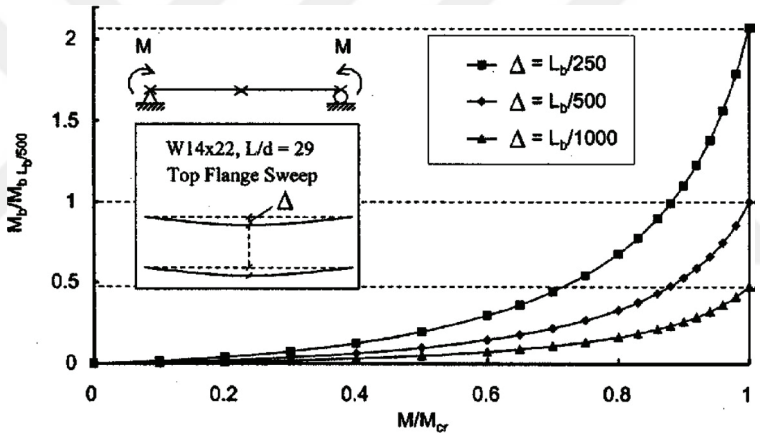

Figure 2. 10. Brace moments versus imperfection magnitude.
(Source: Critical Imperfections for Beam Bracing Systems, Wang and Helwig, 2005)

Wang and Helwig (2005) also studied the distribution of the critical imperfections along the beam and observed that critical initial imperfection takes place closer to the brace near the maximum beam moment point with zero twist at adjacent brace points.

Consequently, the magnitude of the critical imperfection was taken as $L_b/500$ that is imposed in the design of torsional bracing systems in AISC (2001) Specifications.

2.7. Previous Studies

There have been numerous studies during early 1900s on the behaviour of shear diaphragms that are used for stability bracing of beams or girders. It should be noted that an adequate stiffness and strength of the bracing system is crucial for stability of the structures, Winter (1960).

After having unsatisfactory experiences on bridge construction, researchers concentrated on investigation and development of the new bracing sytems to provide stabilization of these structures.

Cornell University have great contributions for understanding the behavior of shear diaphragm used as continuous bracing systems. Errea and Apparao (1976), conducted significiant studies on bracing of I-shaped girders with shear diaphragms. These studies resulted in an energy-based solution for the buckling capacity of girders braced by a shear diaphragm on the compression flange under uniform moment loading.

$$M_{cr} = \sqrt{\left(\frac{n\pi^2 EI_y}{L^2} + Q\right)\left[\frac{\pi^2 EC_w}{L^2} + GJ + Qe^2\right]} + Qe \qquad (2.13)$$

Where,

EI_y = Weak axis bending rigidity;

EC_w = Warping rigidity;

GJ = Torsional rigidity;

e = The distance between the center of gravity of the beam and the plane of the diaphragm;

n = A constant for different end support conditions. (1 for simply supported end and 2 for fixed end.)

The equation above was derived by considering a lateral displacement of compression flange and sinusoidal cross sectional twist along the entire length of the I-girder braced by shear diaphragms on the compression flange.

The expression on the equation (2.2) includes a simple solution suggested by Errera and Apparao (1976) as well as Nethercot and Trahir (1975).

$$M_{cr} = M_g + 2Qe \tag{2.14}$$

where,

Mg = Buckling capacity of the girder alone;

Q = Shear rigidity of the shear diaphragm;

e = Distance from center of gravity of the beam to plane of shear diaphragm.

Helwig and Yura (1999) compared the results of Equation 2.13 and Equation 2.14 by selecting a wide girder section of W30x90 with a span/depth ratio of 20 under uniform loading case and braced by a shear diaphragm. The results of comparison illustrated a well accordance between both of the solutions.

Parameter "e" that is given in Equation 2.13 and Equation 2.14 is defined as the distance between the diaphragm plane and shear centre of the girder by Lawson and Nethercot (1985).

Yet, for transverse loading cases the equation above is not valid. Lawson and Nethercot (1985) derived the following equation for girders subjected to transverse loading cases.

$$M_{cr} = C_b d \left[\frac{\left(Q\frac{(1-g)}{2} - \frac{P_e g}{2} \right) +}{\sqrt{\left(-\frac{P_e g}{2} + Q\frac{(1-g)}{2} \right)^2 - \frac{Q^2}{4} + \left(\frac{P_e}{2} + \frac{Q}{2} \right) \left(\frac{P_e}{2} + 2P_T + \frac{Q}{2} \right)}} \right] \tag{2.15}$$

where,

C_b = Factor for moment gradient;

d = Girder depth;

g = Load height factor;

P_e = Weak axis Euler buckling load;

G = Shear modulus of the beam material;

J = Torsional constant of the beam;

Q = Shear rigidity of the shear diaphragm;

$$P_e = \frac{\pi^2 E I_y}{L^2};$$

$$P_T = \frac{GJ}{d^2}.$$

Lawson and Nethercot (1985) suggested "g" value of 0.45 and 0.55 for uniform distributed load at the top flange and point load at the top flange of mid point of the girder, respectively. When the load height effect "g" is not considered (g = 0) Equation 2.15 yields to Equation 2.16 that resulted in a C_b factor affecting the entire equation.

Helwig and Frank (1999) conducted a numerical study on the contribution of metal deck forms to the stability bracing of steel I-girders. A finite element model is utilized for the investigation. The model was a simply supported twin girder system braced by shear diaphragms a long the length of the girders. The shear diaphragms of the model was created by using four noded shell elements with a unit thickness. Helwig and Frank (1999) altered the modulus of elasticity to modify the shear rigidities of the metal decks to avoid the local buckling problems. The reason to alter the modulus of elasticity instead of the shell thickness was that plate buckling is a linear function of the modulus of elasticity whereas it was a function of the cube of the thickness. So with the use of modulus of elasticity detrimental effect thickness in the third power is avoided. In order to prevent local distortions of the diaphragms, beam elements were used for stiffening the shear diaphragm along panel edges. These beam elements had only out-of-plane stiffeness. Stiffening beams have the corresponding magnitude of moment of inertia as the corrugations of the deck panels. The girders were created from 8 noded shell elements unlike the 4 noded panels. The corners of each deck panel rigidly coupled to center points of the top flange in x, y and z direction for translational degrees of freedoms. The girders were simply supported and free to warp at the supports.

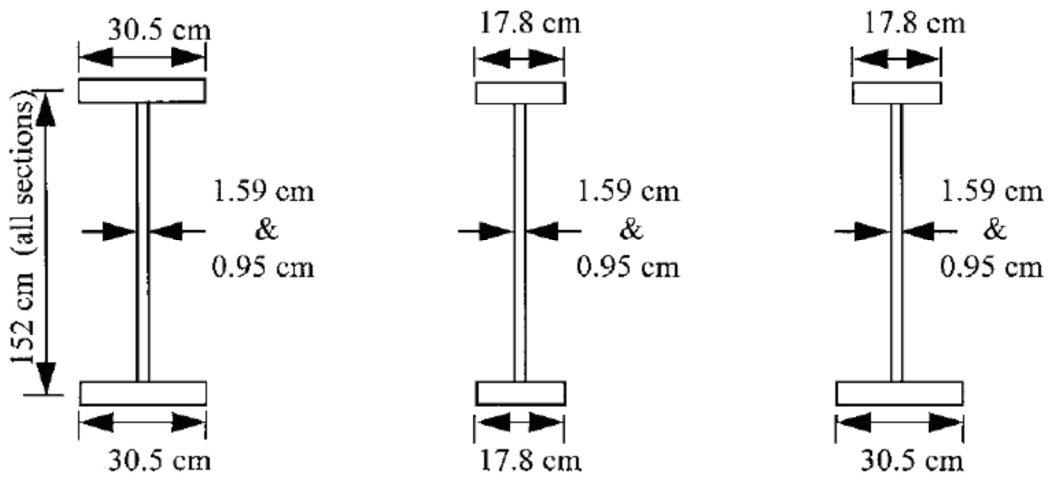

Figure 2. 11. Sections considered in the study of Helwig and Frank (1999).

Web slenderness ratio of the sections was varied from 96 to 160. For each sections, girder span over girder depth values of 10, 20, and 30 were considered. Both singly and doubly symmetric sections were investigated.

Lawson and Nethercot (1985) described the parameter “e” in Equation 2.16 as the distance between geometrical centroid of the section and plane of decking. However, for singly symmetric sections geometrical centroid and shear center does not coincide and can be below or above the mid height of the girder section.

Due to difference in the definition, Helwig and Frank (1999) investigated the effects of “e” on buckling capacity. It was observed that considering “e” as a distance from shear center to plane of decking overestimates the solution. While, as shown in the figure below, considering it as a distance from mid height to plane of decking gives reasonable results.

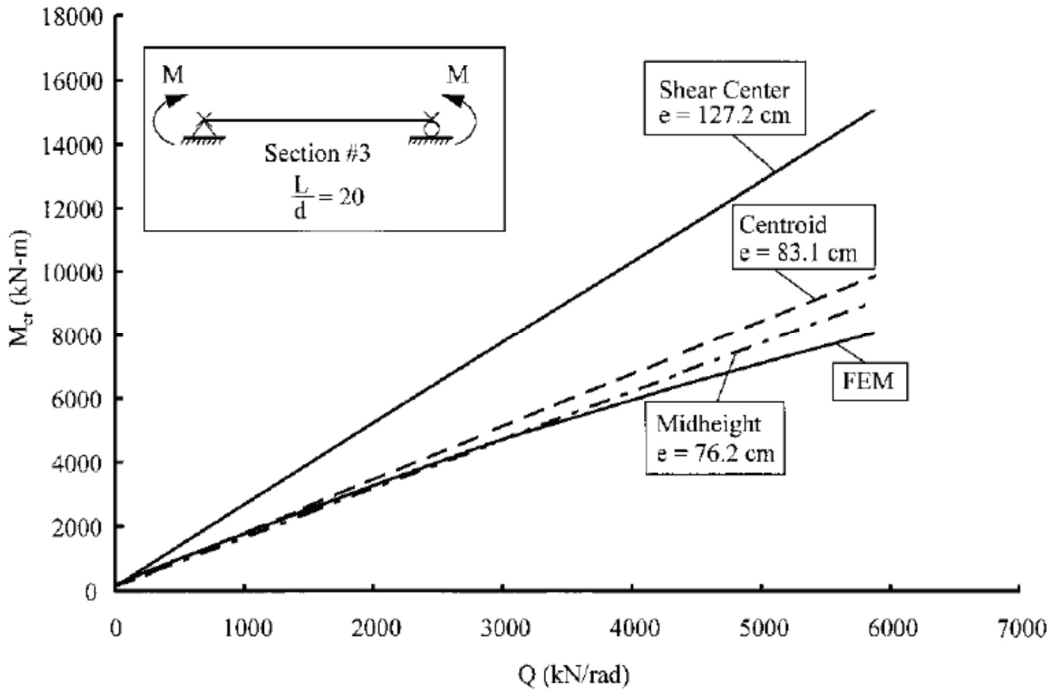

Figure 2. 12. Definition of parameter "e". (Source: Frank and Helwig 1999).

$$M_{cr} = C_b \ (M_g + 2Qe) \tag{2.16}$$

where,

M_{cr} = Buckling capacity of a diaphragm-braced beam;

C_b^* = Moment gradient factor that considers load height effects;

M_g = Buckling capacity of the girder alone;

m = factor for load type and load height effects;

Q = Shear rigidity of the shear diaphragm;

d = Depth of the beam;

Shear rigidity of the deck, Q is calculated as;

$$Q = G' * s_d \tag{2.17a}$$

$$s_d = \frac{n_g - 1}{n_g} * s \tag{2.17b}$$

where,

G' = Effective shear modulus of the diaphragm;

s_d = Tributary width of a diaphragm bracing a single beam;

n_g = Number of girders in the system;

s = Spacing of the girders;

Therefore 2Qe (contribution of the deck to LTB capacity) yields to Qd where d is the depth of the girder. Then Equation 2.16 was modified as below.

$$M_{cr} = C_b \ (M_g + Qd) \tag{2.18}$$

In previous equation moment gradient factor effects the entire buckling equation with girder capacity and deck component together. Thus, finite element analysis results showed that applying C_b factor to the entire equation gives overestimated solutions compared to FEM results. C_b factors of 1.35 and 1.12 were considered for mid span point load and uniformly distrubuted load cases, respectively. Helwig and Frank re-arranged the equation by C_b factor only to the M_g (buckling capacity of a girder alone).

Helwig and Frank (1999) examined the center of twist of the sections to illustrate the decrease in the efficiency of the deck if the moment gradients exists due to the transverse load case, compared to uniform moment loading case.

As mentioned before, the center of twist (COT) which is defined as the intersection of the unbuckled and buckled girder axes, may lie in different positions throught the web. Geometry of the section, type of loading and existence of bracing effects the position of the COT along the girder section.

A closer center of twist to the compression flange of a simply supported I-beam means less effective bracing. Yet as it slides through the top flange, the lateral movement of the top flange will be relatively less even the rigidity of the diaphragms increased. When compared to mid-height loading, top flange loading causes lower buckling capacity of the beam. With their findings, Helwig and Frank (1999) presented that, under uniform loading COT is located below to bottom flange. They also observed that the section subjected to transverse loading at mid height with a moment gradient still has a negative C_T. Negative C_T means that COT is below the bottom flange and positive C_T means that COT is above the bottom flange. C_T implies the distance between the COT and the bottom

flange. Existence of the bracing elevates the COT. Larger shear rigidities results in COT to move closer to the top flange. Therefore over a limit rigidity of the bracing becomes uneffective.

By comparing FEM results with the equation results, Helwig and Frank (1999) figured out that applying C_b to the entire equation (both deck contribution and girder alone) causes over estimation of buckling capacity. There for the C_b factor needs to be applied to the girder alone (M_g) part of the buckling equation. Even in that case, buckling capacity of the system is reported to be still overestimated. Thus a new parameter "m" value is evaluated that accounts for the load height and load type effects and decrease the overestimation of the deck component. Further numerical studies on compact and slender sections with variable L/D ratios are conducted.

As a result of these studies, it is reported that "m" values of 5/8 and 3/8 for mid-height and top flange loading, respectively, could be accepted as reasonable estimates. For top flange loading cases C_b factor requires a simple modification recommended by Helwig et al. (1997) and Galambos (1998). They also modified traditional moment gradient factor C_b for mid-height loading. By accounting for top flange loading effects, moment gradient factor was adopted as $C_b = C_b / 1.4$.

In consideration of these studies, Equation 2.18 modified as follows;

$$M_{cr} = C_b^{*} M_g + mQd \tag{2.19}$$

For a specific design load level (considered as 210 Mpa in the study), or critical buckling capacity, it is possible to obtain ideal rigidity of a shear diaphragm with the transposition of Q_i and rearranging the equation above.

For a continuously braced system, Helwig and Yura (2008a) defined the term "ideal stiffness" as a stiffness that aims a perfectly straight beam to reach a specific load level. Yet the existence of geometrical imperfections on structural members, larger stiffness than the ideal stiffness must be provided to control the deformations. (Winter 1960).

Helwig and Yura (2008-I and 2008-II) conducted analytical studies on stability of a twin-girder decking system braced with shear diaphragms. In these studies, stiffness and strength behaviour of shear diaphragms used to brace stocky beams were investigated. Load type and height effects were also taken into consideration. Helwig and Yura (2008-I) mainly focused on the stability behaviour of the system with a general aspect. The second paper of the study (2008-II) explained the stiffness and strength

requirements of diaphragms and summarizes the design requirements of shear diaphragms.

Helwig and Yura (2008-I) studied on the stiffness requirements of the diaphragms to control deformations of the girders. “m” value in the equation, that is defined by Helwig and Yura (1999), is rearranged for stocky beams. Also cross frames are added at the mid-span to brace the girder and analyses conducted to see its effect on the system. Helwig and Yura (2008-I and 2008-II) considered a predefined initial twist of the beam, as the magnitude of the brace forces is a function of the imperfection of the steel members.

$$\theta_0 = \left(\frac{L_b}{500\,d}\right) \tag{2.20}$$

where,

θ_0 = Initial twist in radians;
L_b = Girder span;
d = Depth of the beam;

Lateral sweep of $L_b/500$ was assumed for the top flange whereas the bottom flange was considered as perfectly straight along the girder length. $L_b/500$ is twice of the value suggested in the Specification for Structural Steel Buildings (AISC 2010a). Helwig and Yura (2008-I) performed eigen-value buckling analyses to determine ideal stiffness of the shear diaphragm for bracing the perfectly straight twin-girder system. In order to determine the strength requirments, they also conducted non-linear statical analyses with large displacements. Shear diaphragms of the model was designed as a truss element as shown Figure 2. 13. Trusses were built up with LINK8 element which is a tension-compression member without bending capabilities and has three degrees of freedom for each node. Shear rigidities of the deck panels were altered by changing the area of the truss members. Results from the truss model and shell model of Helwig and Frank (1999) was compared and the truss model was verified.

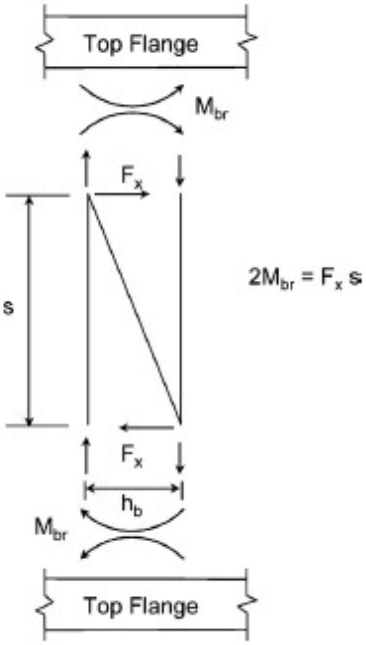

Figure 2. 13. Truss panel model (Source: Helwig and Yura 2008_I).

According to the findings of the study, top flange loading effects were reduced by the existence of discrete bracing. Thus, "m" values evaluated by Helwig and Frank (1999) for slender plate girders before, were reorganised for stocky beams as in the following table.

Table 2. 1. "m" values
(Source: Helwig and Yura 2008a).

	Stocky (h/t_w<60)		*Slender* (h/t_w>60)	
Bracing Condition	Centroid loading	Top flange loading	Centroid loading	Top flange loading
No intermediate discrete bracing	0.85	0.5	0.5	0.375
With intermediate discrete bracing	0.85	0.85	0.5	0.375

Helwig and Yura (2008a) conducted large displacement non-linear analyses on initially imperfect twin girder system braced by shear diaphragms. They reported that transverse loads applied at the centroid resulted in smaller maximum brace forces than uniform moment loading. Applying loads on top flange increased the maximum brace

force and top flange transverse loading elevated the maximum brace forces regardless the load type. The maximum mid-span rotations were obtained for transverse loading at top flange case and minimum rotations were obtained for uniform moment loading case. Adding intermediate cross frames at the mid-girder caused reduction in both rotations and brace forces as it brace the girders and reduce the span. As a result, providing a rigidity value of four times the ideal shear rigidity provides reasonable results to control the rotations and brace forces when compared to two and six times of it. Since the effect of shear rigidity got smaller, increasing it to six times become ineffective. Thus, Helwig and Yura (2008a) suggested to use four times the ideal shear rigidity value.

$$Q_{req} = 4 * Q_i = 4 \frac{M_u - C_b^* M_g}{md} \tag{2.21}$$

where,

M_u = Maximum design moment of a diaphragm-braced beam;
C_b^* = Moment gradient factor that considers load height effects;
M_g = Buckling capacity of the girder alone;
m = factor for load type and load height effects;
Q = Shear rigidity of the shear diaphragm;
d = Depth of the beam;

Helwig and Yura (2008b) concentrated on obtaining stiffness and strength requirements for shear diaphragm that are used to brace stocky beams.

Helwig & Yura (2008b) performed large displacement analyses on stocky beams and proposed the brace forces along length of the beam M_{br}' as seen in Figure 2. 14. As a result, Helwig and Yura (2008b) recommended the following equation for M_{br}'.

$$M_{br}' = 0.001 \frac{M_u L}{d^2} \tag{2.22}$$

where,

M_u = Maximum design moment of a diaphragm-braced beam;

M_{br}' = Warping restraining moment per unit length along the longitudinal axis of the beam;

L = Spacing between bracing points;

d = Beam depth.

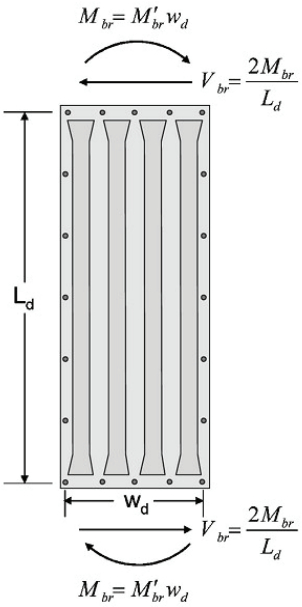

Figure 2. 14. Brace moment and shear on corrugated sheet.
(Source: Helwig & Yura, 2008-II)

In Figure 2. 14 each decking sheet is fastened at both edge and at the side lap fasteners. Edge fasteners were used to connect corrugated sheets to girder elements while side lap fastener were used to connect adjacent decking sheets. Helwig and Yura (2008b) assumed that edge fasteners, used to connect the sheet with the girder, equally resist to the shear forces generated in the shear diaphragm. Thus, they transformed the brace moment per unit length M_{br}', M_{br} moment of a decking sheet formulated in Figure 2. 9. From equilibrium, Helwig & Yura (2008-II) presented the following equations for the shear force components in an edge fastener.

$$F_v = \frac{V_{br}}{n_e} = \frac{2M_{br}}{L_d n_e} = \frac{2M_{br}' w_d}{L_d n_e} = 2\left(0.001\frac{M_u L w_d}{L_d n_e d^2}\right) \tag{2.23}$$

$$F_M = \left(0.001\frac{M_u L}{1.25d^2}\right) \tag{2.24}$$

$$F_R = \sqrt{F_M{}^2 + F_V{}^2} \tag{2.25}$$

where,

F_V = Component of brace force parallel to beam longitudinal axis;

F_M = Component of brace force perpendicular to beam longitudinal axis;

F_R = The resultant force in fasteners;

V_{br} = Shear force in truss panel;

n_e = Number of edge fasteners per panel;

M_{br} = Brace moment in diaphragm truss panel;

M_{br}' = Warping restraining moment per unit length along the longitudinal axis of the beam;

L_d = Spacing between bracing points;

w_d = width of the shear diaphragm;

M_u = Maximum design moment of a diaphragm-braced beam;

L = Span of the beam;

d = Beam depth.

CHAPTER 3

FINITE ELEMENT MODEL

3.1. Introduction

The three dimensional finite element program ANSYS (2007) was utilized to conduct the analytical studies on the lateral torsional buckling behavior of the twin steel I-girder and beam system braced by shear diaphragms. The finite element model of the system consists of three different element types in order to simulate an analogous behavior with the real life applications. Material nonlinearity was not taken into consideration in the model and all of the elements have linearly elastic material properties. The model of the twin-girder system braced with a corrugated metal deck form is depicted in Figure 3. 1. The ANSYS finite element model was composed of 8 noded-shell elements (SHELL93) to simulate steel I-girders or beams and web stiffeners, 3-D truss elements (LINK8) to simulate the metal deck forms and spring-damper elements (COMBIN14) to simulate the screws that fasten the thin elements to heavier structural units. For stitch connections between sheets at the side-laps, 3-D truss elements were used by providing the equivalent lumped stiffness of the side-lap fasteners. 3-D truss elements have only uniaxial compression and tension behavior.

In this chapter, finite element models of steel I-beams, metal decks, fasteners and cantilever shear frame are presented respectively. Furthermore, verification of finite element model is also adverted.

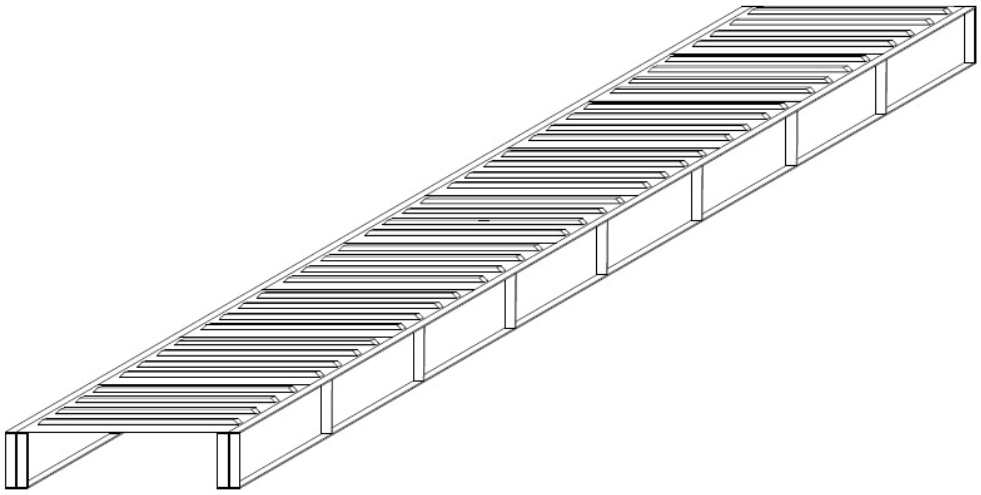

Figure 3. 1. Twin girder and metal deck diaphragm system.

3.2. Finite Element Model and the Loading Procedure

Non-linear static analyses are conducted to observe the stiffness requirements of I-beams that are braced with the permanent metal deck forms. In the model, geometrical non-linearity are considered but material non-linearity was ignored. Girders are loaded in gravitational direction at each mid-node of the top flange along the girder with uniform distributed loading. Laboratory tests of twin girder system braced by metal decks indicate that girders have maximum bending stress level of 210 MPa at the extreme fiber. (Egilmez et. al, 2007). Thus, load level are selected to provide such a stress level. Loading is completed in twelve steps. Twenty percent of the total loading is applied in first three steps. Ten percent increment in two steps, five percent increment in two steps and two percent increment in five steps followed the initial loading. Each loading phase has 105 sub steps. In the sub steps, convergence criteria for force, moment and displacement are checked and verified through iterations. These criteria are set 0.1% and 1% for force/moments and displacements respectively. Some of the analyses are terminated due to low convergence criteria or due to large deformations and instability of the girders.

3.3. FEA Model of Steel I-Girders

The beam and girder elements and web stiffeners are meshed with 8-noded quadrilateral shell elements which are referred as SHELL93 in ANSYS element library (2007). For structural mechanic problems, SHELL93 element demonstrated in Figure 3. 2 could be a proper selection to model curved shells. The element has six degrees of freedom at each node: translations in the nodal x, y, and z directions and rotations about the nodal x, y, and z-axes and has quadratic deformation shapes in both in-plane directions. Large deformation capability of the element is an advantage for the accuracy of nonlinear analyses.

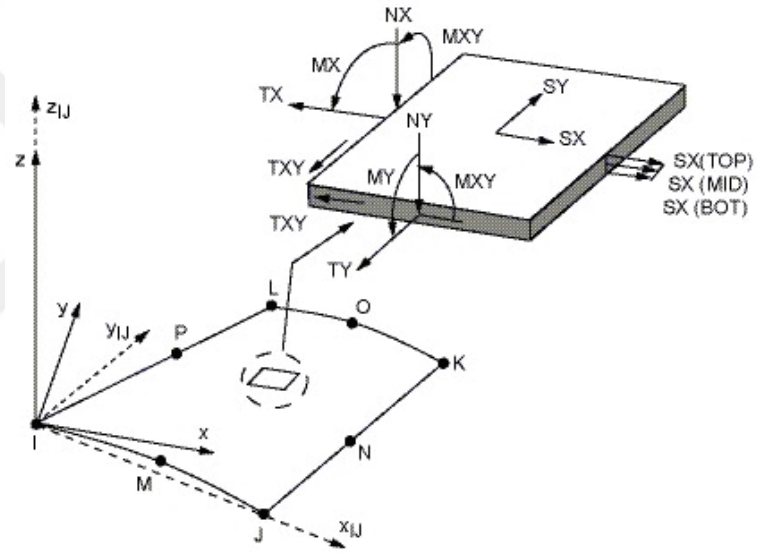

Figure 3. 2. SHELL93 Element in ANSYS library.

Table 3. 1. Material Properties of ASTM A992-Grade 345 Mpa Steel.

Modulus of Elasticity (Mpa)	=	205000
Shear Modulus (Mpa)	=	78800
Poisson's ratio (ν)	=	0.30

Material properties defined in Table 3. 1 were assigned to shell elements (SHELL93) that generates girders and web stiffeners.

Flanges of the steel-I beams or girders were divided into two shell elements. Either side of the flange center possesses one shell while the numbers of elements along the web depth are four. The sensivity of the model and the fineness of the meshes were checked by increasing the element number to eight at the web. It was observed that increasing the element number did not have a significiant effect on the accuracy of the model. In comparison with the web that consists four elements, results were close and in both cases excessive distortions of elements were avoided. Thus, webs were divided into four elements to reduce the degrees of freedom and correspondingly the elapsed time of the anlyses. Aspect ratios of shells were maintained below. It should be noted that the web and flange common nodes were rigidly coupled.

Merely, uniformly distributed loading case was considered since it reflects the real life loading conditions and represents loading of pour concrete slab. Midspan point load case was not considered. Thus, sections with compact webs had vertical web stiffeners only at their supports to eliminate the local effects. However sections with slender webs had transverse stiffeners at their supports and every defined space, 'a', which varies according to girder depth, 'h'. The 'a/h' ratio is kept constant and approximately equal to one. Dimensions of the web stiffeners is selected based on the width of the flange and the depth of the web. Thicknesses of the web stiffeners are all same and equal to 20 mm. Figure 3. 3 illustrates an imperfect girder that is modeled with ANSYS without boundary conditions and applied forces on it. Note that the stiffeners are presented in the figure.

The beams or girders were simply supported. The lateral movements at the supports were prevented at the top and bottom flanges. The web was free to warp to provide free rotations of the metal decks.

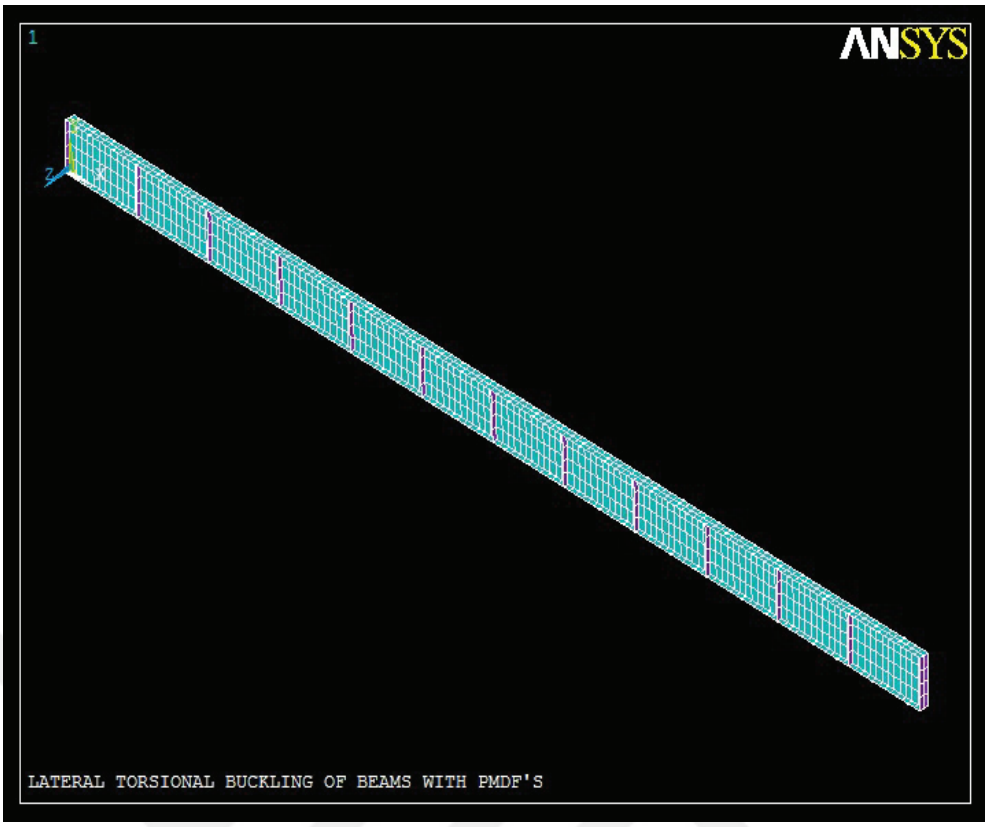

Figure 3. 3. ANSYS FE Model of the girders and beams.

The initial geometry of a structural member in the system effects the bracing behavior and the buckling capacity, because an imperfect element could not reach the load carrying level of a perfectly straight member. Thus, initial imperfections play an important role in the magnitude of brace forces that develop in bracing members. Wang and Helwig (2005) showed that the brace forces are directly proportional to the magnitude of initial imperfections for beams braced by cross frames or diaphragms. Wang and Helwig (2005) also showed that the worst-case imperfection for maximizing brace forces forms by the lateral sweep of the compression flange while the tension flange remains essentially straight. For the magnitude of lateral sweep of the top flange, both Wang and Helwig (2005) and Helwig and Frank (2008a) suggested using $L_b/500$ instead of the 1/1000 limit set by the AISC Code of Standard Practice (AISC 2010) on the variation in straightness between points of lateral supports in bridge applications. The reason for doubling the magnitude of lateral sweep is due to possible additional out-of-plumpness and uneven bearing supports in bridge constructions, which may result in larger imperfections. The shape and magnitude recommended by Wang and Helwig (2005) and Helwig and Yura (2008a) for initial imperfections is adopted in this study. The geometry

and the values of these imperfections are shown in Figure 3. 4 and 3.5. The corresponding approximate initial twist is expressed in the following expression. Geometric imperfection of the beams were introduced to the analyses through modeling the beam geometry.

$$\theta_0 = \frac{L_b}{500d} \tag{3.1}$$

where: L_b = unbraced length of the beam and d= depth of beam.

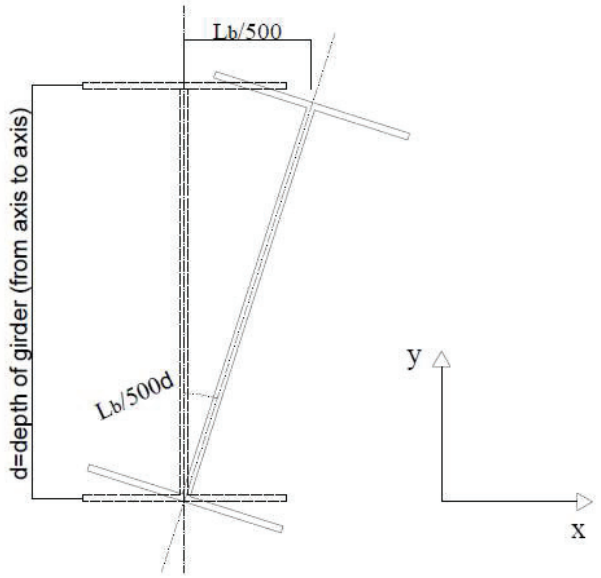

Figure 3. 4. The shape and magnitude of imperfections used in the study.

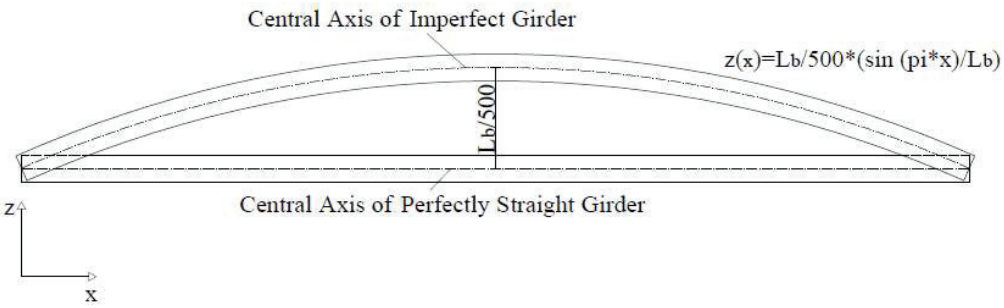

Figure 3. 5. Plan view of imperfections.

3.4. FEA Model of Shear Diaphragm

The FEA model used for shear diaphragms was adapted from a study by Davies and Bryan (1982). In this study, Davies and Bryan (1982) simulated the shear stiffness of diaphragms by a series of bars forming a truss. Each small truss shown in Figure 3. 6 consists of four transverse and three diagonal truss elements and represents a single deck sheet profile. The deck sheet profile modeled in this study is a deck sheet with three corrugations commonly used in both building and bridge applications.

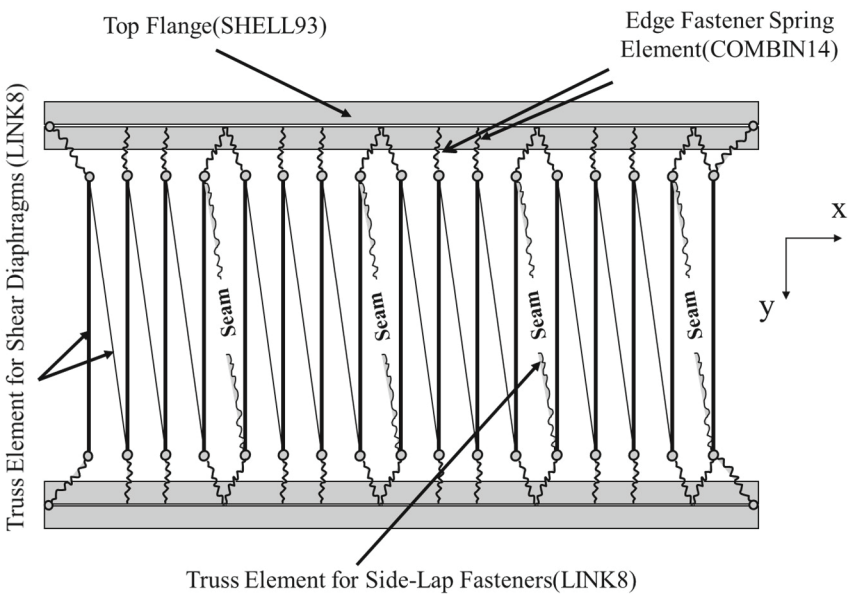

Figure 3. 6. Analytical model of twin girder system based on Davies and Bryan.

The sub-model used for deck sheet is presented in Figure 3. 7. The transverse truss elements are located at every trough and span between the centerline of beam top flanges. This type of a representation of deck sheets enables the deck to structural member (twin beams in this study) fastener to be modeled by dimensionless spring elements and be placed at the ends of each transverse truss element. The transverse truss elements were connected to the beam top flange mid-nodes through these dimensionless spring elements. The number of transverse truss elements can be changed depending on the number of fasteners used to connect the deck sheet to structural member. The truss elements are 3-D uniaxial tension-compression bar elements. The axial stiffness of the transverse elements is taken sufficiently high to be able to neglect the axial strain. Hence, the shear

stiffness of the deck sheets depends only on the properties of the diagonal elements. In order to determine the required area of the diagonal truss elements that corresponds to a certain shear rigidity, an FEA model of an existed shear test frame was utilized.

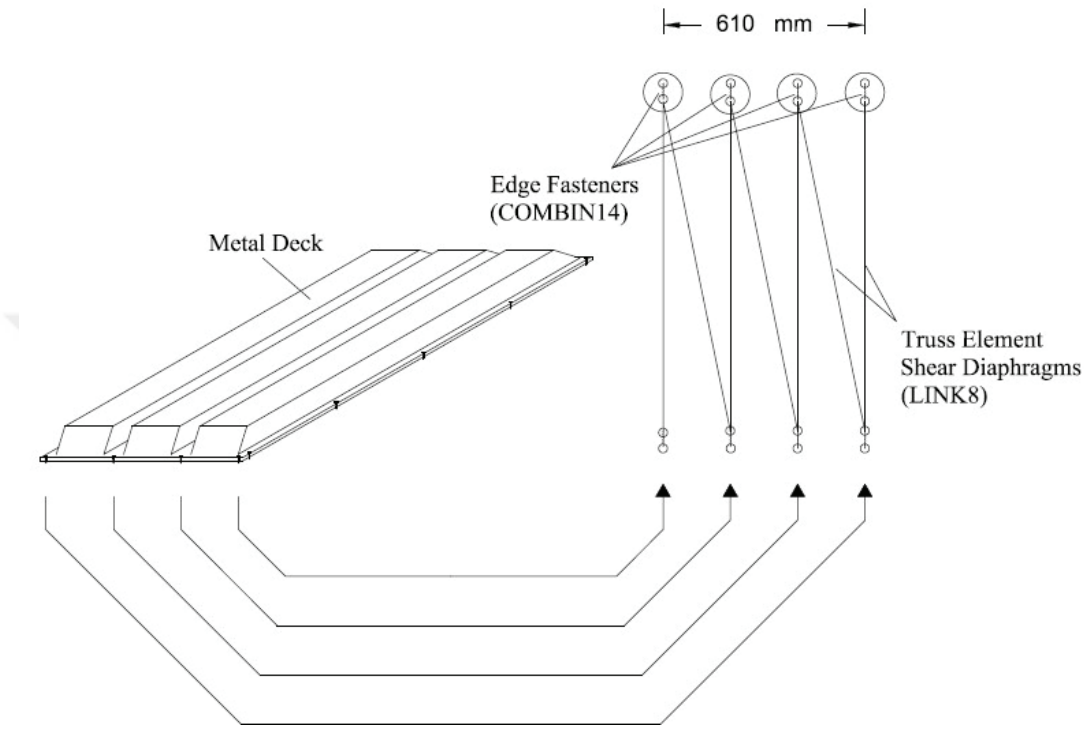

Figure 3. 7. Finite element analytical model of a metal deck.

3.5. FEA Model of Fasteners

Luthrell (2004) stated that stiffness and strength of a connection between the metal deck and the structural member depend on the diaphragm properties, span arrangements and the quality of the connection. Connections can be established by welds, screws or power driven pins. In building and bridge applications, deck sheets are generally fastened to supporting members along the edges at every trough and to each other at side-lap locations by mechanical fasteners. Conventional mechanical fasteners for deck sheets are generally 19 mm (¾ in) long TEKS screws with a 6.3 mm (¼ in) diameter. In this study, the fasteners that connect deck sheets to supporting members were modeled by dimensionless spring elements that possess equal stiffness in two orthogonal directions, but no rotational and bending stiffness. COMBIN14 element in ANSYS library was

chosen to simulate the flexible screw connection. COMBIN14 element provides a uniaxial tension-compression behavior with three degrees of freedoms for each node that consists of translation in x, y and z directions.

Figure 3. 8. LINK8 geometry and stress output.
(Source: ANSYS 14 Documentation.)

COMBIN14 elements were positioned at the centerline of beam top flanges and connected to the mid-node of beam top flanges and the ends of the transverse truss elements. General layout of fasteners can be seen in Figure 3. 6 on the previous page. Although the dimensionless spring elements are demonstrated with a finite length in Figure 3. 9, this representation is merely for illustration purposes.

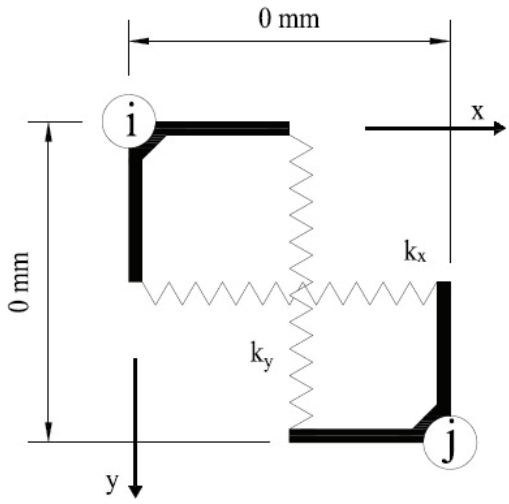

Figure 3. 9. FE model of the fastener based on Davies and Bryan.

At side-lap locations separate spring elements were used to connect each transverse truss end to the same mid-node of beam top flange. The transverse and lateral stiffness of these dimensionless spring elements were assumed to be the same as the stiffness of No. 12 and No. 14 Buildex TEKS screws used to develop the SDI Design Manual (Luthrell 2004) equations. For the stiffness of deck to structural member connections, SDI Design Manual (Luthrell 2004) recommends the following expression:

$$k_{structural} = \frac{10^6 \sqrt{t}}{37.4} \quad N/mm \tag{3.2}$$

where: t = thickness of sheet metal

In the shear diaphragm bracing composition, panels adjacent to the supports are assumed to be fastened to structural members (beam, diaphragm, etc.) that span transversely between the supports. An example of the current application is given in Figure 3. 10.

Figure 3. 10. Transverse diaphragm at the supports.

The stiffness of the deck to structural member connections is also considered and incorporated in the model by providing additional spring elements that connect the corner node of the deck trusses adjacent to the supports.

Deck to deck connections, in other words side-lap connections were modeled by a transverse truss element that connects opposite edges of adjacent small trusses as shown in Figure 3. 10. The stiffness of the side-lap transverse truss elements consisted of the sum of the stiffness of the total number of fasteners used at side-lap connections. According to Permanent Metal Deck Form (PMDF) standards by Texas Department of Transportation (TxDOT 2004) a maximum center-to-center spacing of 450 mm (18 in) is required at side-laps. The stiffness of a deck to deck connection was calculated according to the SDI Design Manual (Luthrell 2004):

$$k_{side-lap} = \frac{10^6 \sqrt{t}}{86.3} \quad N/mm \tag{3.3}$$

where: t has been defined in Eq. (3.2).

The number of fasteners at deck to beam connections considered in this study ranged from five to three. The number of fasteners at deck to deck connections ranged from six to four. A standard deck with dimensions 610 mm and 2750 mm was used. These dimensions are representative of practical deck lengths utilized in both the building and bridge industries.

As can be seen from Eq's. (3.2) and (3.3) both the deck to structural member and deck to deck connection stifness depend on the thickness of the deck sheet. In order to investigate the effect of sheet thickness on fastener forces, three different deck thicknesses (0.91, 1.22, and 1.52 mm [20, 18, and 16 ga.]) were considered in this study.

3.6. The FEA Model of Shear Frame

Prior to buckling and large deformation analyses, it was crucial to obtain the shear stiffness values of the system that brace the steel I-beams or girders. For this purpose, shear frame analyses were utilized to measure shear characteristics of metal decks. In Figure 3. 11, FE model of shear frame is demonstrated. The model consists of two

adequately rigid beams (BEAM3), 3-D truss elements to generate shear diaphragms (LINK8), dimensionless spring elements (COMBIN14), and at the end a rigid link element to provide load transfer. Translation of beams is restricted in both x and y directions at supports. The system has 8 deck members. The frame is restrained at the left end. The other end is not supported and free to deform. The shear diaphragm created in the cantilever shear frame model involves all the properties of metal decks defined in the previous paragraphs. The same model for metal deck will be utilized in eigenvalue buckling and large deformation analyses.

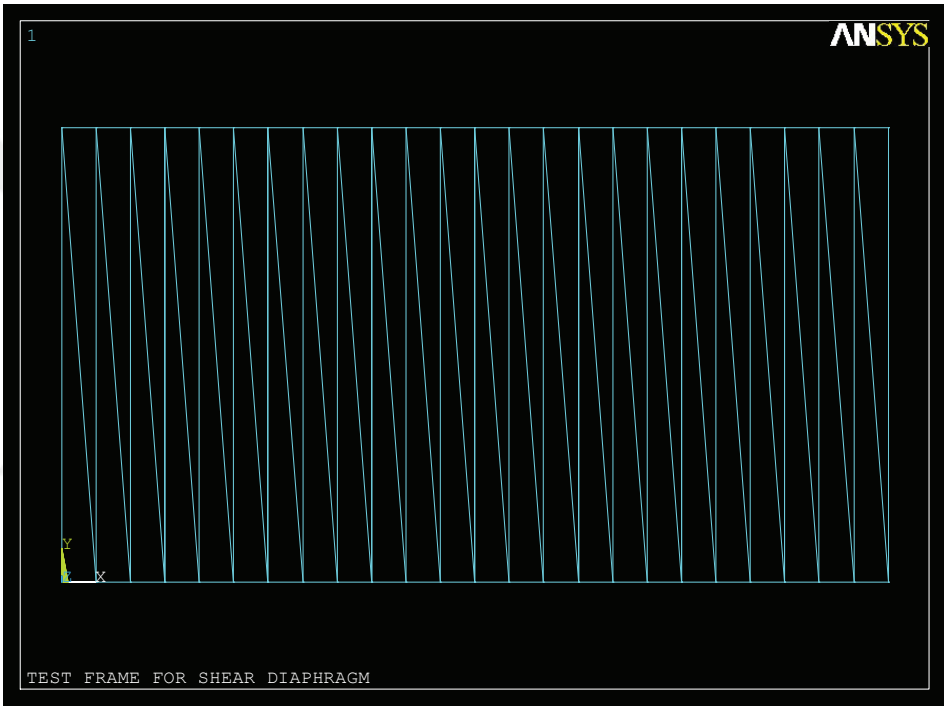

Figure 3. 11. FE model of shear frame used to measure shear parameters.

The main target of shear frame analyses was to obtain the area of diagonal truss elements to determine shear rigidities of the metal decks. Altering these areas provides the necessary shear stiffness values of the system. Vertical truss elements have high axial rigidities and have no influence on determination of the shear rigidity. Truss representation of metal deck eliminates the local distortions of the diaphragm.

3.7. Verification of the FEA Model

The FEA simulation was verified by comparing the buckling behavior of a 14.63 m (48 ft) twin-girder system braced by permanent metal deck forms (PMDF). The test used in the verification study was a full-scale twin-girder buckling test conducted at the structural engineering laboratory of University of Houston. The girders were US wide flange beams, W760×134 (US: W30×90), with a depth of 753 mm and web thickness of 15.5 mm. The top flanges of the girders were flame cut from the original 264.2 mm (10.4 in) width to 158.8 mm (6.25 in) to produce a singly symmetric section with $\rho=I_{yc}/I_y=0.18$; where I_{yc} and I_y are respective moment of inertias of the compression flange and the entire cross section about a vertical axis through the web. Point loads were applied to the girders through two gravity load simulators at third points. The deck form system used in the test set-up represented a forming system used in the bridge industry with a modified connection detail. The 1.22 mm (18 ga) thick PMDF sheets were 610 mm wide and were supported on cold-formed L76×51×3.3 mm (L3×2 10 ga) galvanized angles. The modified connection detail consisted of transverse stiffening angles that spanned between the top flanges of the girders. The spacing of the stiffening angles was 4.88 m (16 ft). A full description of the test set-up is given by Egilmez et. al (2012). The effective shear stiffness of the deck form system was measured to be 7184 kN/m-rad; which corresponded to a deck shear rigidity of 9842 kN/rad (Egilmez et. al, 2007). The 9842 kN/rad shear rigidity corresponded to approximately 5.4 times the ideal shear rigidity of the deck system for a stress level of 210 MPa (30.43 ksi).

Figure 3. 12 presents the comparison of the test results and the FEA simulation for mid-span moment vs. mid-span total twist/initial twist. It can be seen from the figure that the FEA model predicted the behavior of the test beam satisfactorily in the elastic region. The rotations of the FEA model were approximately 4.7% higher than the rotations of the girders observed in the test. Since elastic materials were used in the FEA model, it was not possible to simulate the inelastic behavior of the twin-girder system.

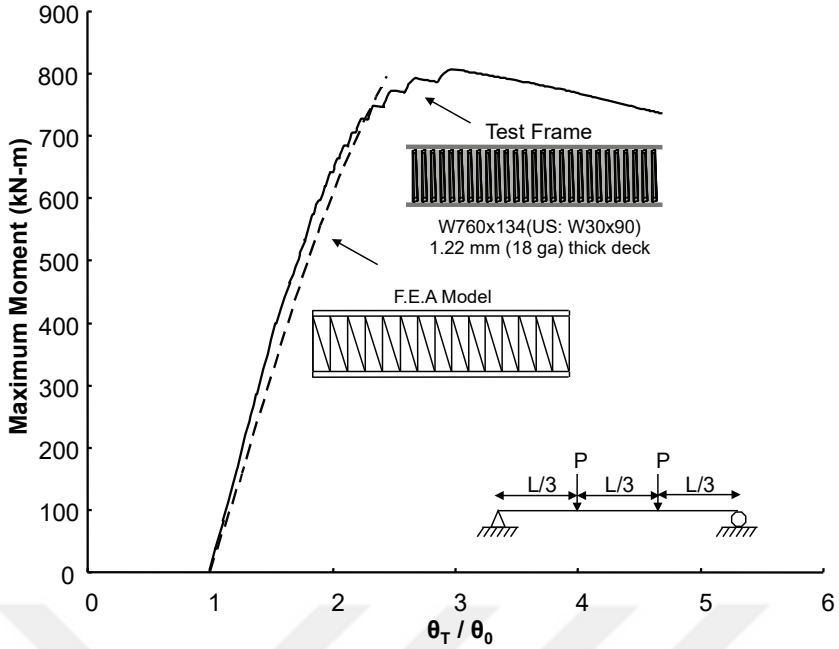

Figure 3. 12. Comparison of FEM and laboratory test results (Source: Egilmez et. al, 2012).

CHAPTER 4

OVERVIEW OF STUDY

4.1. Introduction

In this chapter, overview of the study is presented. The presentation consists of the procedure to obtain the stiffness requirements of the decks, the definition of the selected cross sections and the parameters of the analysis that are used in the study.

The study involves an eigenvalue buckling analyses in order to obtain ideal shear rigidities of the twin girder system, a shear frame analyses to define the areas of diagonal truss members in the deck model and a large displacement static analyses to investigate the stiffness requirements of the shear diaphragms. ANSYS Mechanical APDL (2007) was utilized to perform the analyses. In order to investigate the stiffness requirements of the shear diaphragms, the rotation of the cross section around x-axis at mid-span, the brace forces developed in the edge and side lap fasteners were examined.

4.2. Analysis Parameters

It is known that efficient sizing of the web and the flanges could provide economical solutions. The flanges essentially resists the bending, torsional forces while the web principally resists the shear forces. It is obvious that the width of the flanges have an influence on the lateral torsional buckling behavior of the section, therefore necessary consideration should be given to this in the design of the flanges. Narrow flange widths increase the sensitivity of the member to lateral torsional buckling. Such a selection necessitates the investigation of its effects on the stiffness and strength of requirements of the shear diaphragms. It is known that extremely narrow width of the flanges could cause convergence problems in non-linear analyses due to instability of the girders resulting from high lateral displacements. Therefore, in this study the flange widths of the beams were selected to avoid such an instability. Flange width is controlled by the h/b ratio in the study. This same ratio is named as cross-section aspect ratio in AASHTO

LRFD 2012 Bridge Design Specifications 6th Edition. Figure 4. 3 tabulates the section designations and cross sectional properties of the beams selected for the study. The beam sections consisted of six doubly symmetric and six singly symmetric sections. The web slenderness ratios (WSR) of doubly symmetric sections were 60, 100, and 160; whereas for singly symmetric sections WSR were 100 and 160. The depths of sections with WSR of 60 were 366 mm (14.4 in) and 732 mm (28.8 in) and are referred to as Stocky#1, and Stocky #2, respectively. Flange widths of the stocky beams were respectively 140 mm (5.5 in), and 280 mm (11 in). Flange slenderness ratios (FSR) of these two stocky beams were 7.78. Sections with WSR of 100 and 160 are referred to as DS Slender 100#1 and 160#1, and DS Slender 100#2 and 160#2. The depth of Slender-100 and 160 sections were 1464 mm (57.6 in) and 1830 mm (73.71 in). For the four slender sections flange widths were considered: 300 mm (11.8 in). FSR of the slender sections were six.

In addition to doubly symmetric sections, six singly symmetric sections, referred as SS Slender 100#19 to SS Slender 160#39, were also considered. The sections had a depth of 1464 mm and 1830 mm, a bottom flange width of 300 mm (11.8 in). The FSR of this sections is 6. Top flange widths of the sections were altered to achieve ratios of mono-symmetry (I_{yc}/I_y) of 0.19 (SS-Slender 100#19 and SS Slender 160#19), 0.29 (Slender 100#29 and SS Slender 160#29), and 0.39 (SS Slender 100#39 and SS Slender 160#39); where I_{yc} is the weak axis moment of inertia of the compression flange and I_y weak axis moment of inertia of the entire cross-section. The AASHTO Standard Specifications (2010) requires the ratio of mono-symmetry to be within the following limits: $0.1 \leq I_{yc}/I_y \leq 0.9$. Figure 4. 3 demonstrates typical geometry of the cross-sections analyzed in this study. In Table 4. 2, web and flange slenderness ratios of the sections and the aspect ratios of the mesh elements were given. In Figure 4. 1 and Figure 4. 2 illustrates the cross sections analyzed in this study.

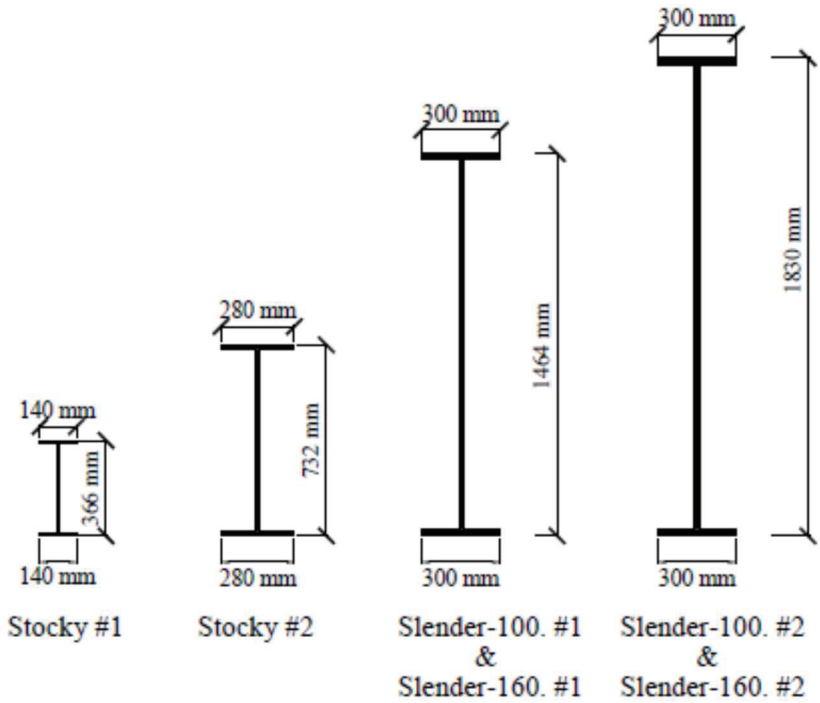

Figure 4. 1. Doubly Symmetric Sections analyzed in the study.

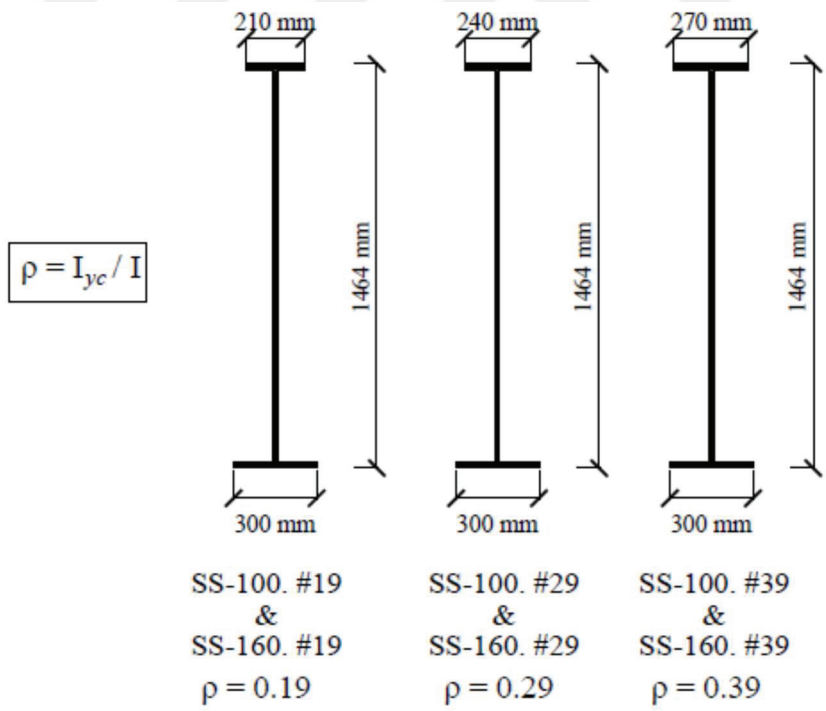

Figure 4. 2. Singly Symmetric Sections analyzed in the study.

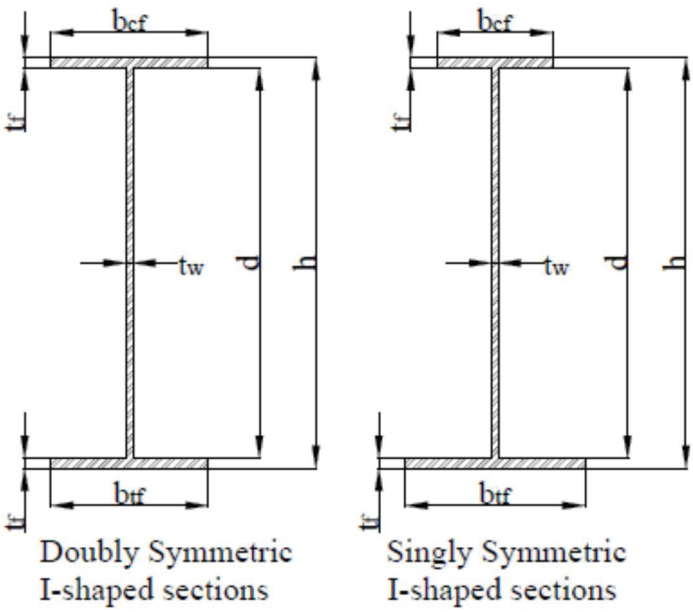

Figure 4. 3. General geometry of steel I-beams and girders.

Table 4. 1. Sections to be analysed in the study.

		Flange				Web	
Sections	**Class**	**Width of Top Flange (b_{cf}) mm**	**Width of Bottom Flange (b_{tf}) mm**	**Thickness (t_{cf}) mm**	**Thickness (t_{tf}) mm**	**Height (h) mm**	**Thickness (t_w) mm**
Doubly Symmetric I-Shaped Girders							
Stocky #1	Compact	140	140	9.00	9.00	366	6.00
Stocky #2	Compact	280	280	18.00	18.00	732	12.00
DS Slender 100#1	Slender	300	300	25.00	25.00	1464	14.14
DS Slender 160#1	Slender	300	300	25.00	25.00	1464	8.84
DS Slender 100#2	Slender	300	300	25.00	25.00	1830	17.80
DS Slender 160#2	Slender	300	300	25.00	25.00	1830	11.13
Singly Symmetric I-Shaped Girders							
SS Slender 100#19	Slender	210	300	17.50	25.00	1464	14.21
SS Slender 100#29	Slender	240	300	20.00	25.00	1464	14.19
SS Slender 100#39	Slender	270	300	22.50	25.00	1464	14.16
SS Slender 160#19	Slender	210	300	17.50	25.00	1464	8.88
SS Slender 160#29	Slender	240	300	20.00	25.00	1464	8.87
SS Slender 160#39	Slender	270	300	22.50	25.00	1464	8.85

Table 4. 2. Slenderness and aspect ratios of webs and flanges.

Sections	Class	Flange Slenderness Ratios ($\lambda_{fTOP}=b/2t_{cf}$)	Flange Slenderness Ratios ($\lambda_{wBOT}=b/2t_{tf}$)	Web Slenderness Ratios (h/t_w)	Aspect Ratios Flanges Top	Aspect Ratios Flanges Bottom	Aspect Ratios Web
Doubly Symmetric I-Shaped Girders							
Stocky #1	Compact	7.78	7.78	58.00	2.90	2.90	2.34
Stocky #2	Compact	7.78	7.78	58.00	1.45	1.45	1.17
DS Slender 100#1	Slender	6.00	6.00	100.00	1.36	1.36	1.74
DS Slender 160#1	Slender	6.00	6.00	159.95	1.36	1.36	1.74
DS Slender 100#2	Slender	6.00	6.00	100.00	1.36	1.36	2.19
DS Slender 160#2	Slender	6.00	6.00	159.93	1.36	1.36	2.19
Singly Symmetric I-Shaped Girders							
SS Slender 100#19	Slender	6.00	6.00	100.04	1.94	1.36	1.75
SS Slender 100#29	Slender	6.00	6.00	100.00	1.69	1.36	1.74
SS Slender 100#39	Slender	6.00	6.00	100.04	1.51	1.36	1.74
SS Slender 160#19	Slender	6.00	6.00	160.08	1.94	1.36	1.75
SS Slender 160#29	Slender	6.00	6.00	159.98	1.69	1.36	1.74
SS Slender 160#39	Slender	6.00	6.00	160.06	1.51	1.36	1.74

For stocky sections, span-to-depth ratios (*L/d*) of 15, 20, 25, and 30 were considered. Also, the L/d ratios for the slender and singly symmetric sections were 10 and 15.

The only loading condition considered was uniformly distributed load applied at the top flange. It is selected due to the fact that uniformly distributed loading is representative of loading for newly poured concrete slab. The level of uniformly distributed load considered in the study results in 210 MPa bending stress at the extreme fiber. This magnitude of loading is accepted to give a reasonable assessment of the stress that is expected in the construction phase. Noting that applied loading resulted flexure in the girders, the flexural effects, F2 and F5 parts of Chapter F (Design of Members for Flexure) in AISC (2010) must be satisfied for the defined limit states. In addition to Chapter F, due to shear effects, slender webs and webs under concentrated load on supports should be satisfied according to requirements of Chapter G (Design of Members for Shear). For this purpose, transverse web stiffeners were attached to the webs of the slender beams along the girder. Stocky beams possess web stiffeners at only supports. These stiffeners were placed with a distance equals to beam height. Thickness of the web stiffeners were 20 mm for all sections. Loading applied at mid-height was not considered since it is less critical as compared to top flange loading (Helwig and Yura, 2008a and b).

The stiffness of a brace system has a significant effect in controlling deformations and reducing the brace forces. In literature, the magnitude of required brace stiffness has generally been defined as a function of the "ideal stiffness" of the brace. As previously mentioned, the "ideal stiffness" corresponds to the brace stiffness required for a structural member to reach a specific load level. A brace stiffness higher than the ideal stiffness is need to control deformations and brace forces. In previous studies, brace stiffness recommendations for column and beam bracing systems generally varied between twice to four times of the "ideal stiffness", respectively; depending on the braced member and the bracing type (Yura 2001, Helwig and Yura 2008a). These recommendations are generally based on a philosophy to provide a brace stiffness large enough to limit the brace forces to reasonable values. The magnitude of a reasonable brace force is somewhat arbitrary; however, it has been depicted that limiting the total amount of deformations at the design load to be around twice to four times the initial imperfections was usually sufficient to control the magnitude of brace forces (Yura 2001, Helwig and Yura 2008a).

The failure of the shear diaphragms is largely controlled by either the edge fastener capacity or side lap fastener capacities (Luthrell 1981, Davies and Bryans, 19982). The capacity of fastener is a direct function of the thickness of the decks. In this study, deck thickness is taken as 1.52 mm (16 ga) which provide reasonable brace forces for fastener.

Rigidity of the diaphragm is a key parameter of the study. As mentioned before, system demands a shear diaphragm rigidity larger than the ideal value. Thus, twice ($2Q_i$) to four times ($4Q_i$) of ideal shear rigidity of the shear diaphragm was taken. Standard deck configuration has four edge fasteners and five side lap connection fasteners. Deck width of the study is 610 mm.

4.3. Procedures of the Numerical Study

First step of the numerical procedure was the creating the mathematical model of the twin girder system. Definition of the girder was followed by the modelling of the shear diaphragm and edge and side lap fasteners. Afterwards, the load values on each node, that are necessary to simulate uniformly distributed loading to cause 210 MPa bending stress at the extreme fiber, were calculated.

Initially, ideal shear rigidities were calculated by conducting eigenvalue buckling analyses on perfectly straight twin girder system braced by shear diaphragms. In eigenvalue buckling analyses, the area of the diagonal truss elements of shear diaphragm was incrementally modified until reaching the specified buckling load level. The purpose was to reach the 210 MPa stress level at the extreme fiber of the cross section at mid-span. After reaching the target factored load, the area of the diagonal truss member was noted to be used in shear frame analyses later. By utilizing the equations 4.1and 4.3, ideal shear rigidity of the system was obtained.

Considering the initial imperfections, it is obvious that the decking system will not reach M_{cr}. Thus, a larger value of brace stiffness must be provided to control deformations and brace forces (Winter 1960; Yura 2001). For this purpose two to five times of ideal shear rigidities were considered.

Thereafter obtaining all the required shear stiffness values, areas of the diagonal truss members were computed by using the shear frame analyses and the equations 4.1 and 4.3. Figure 4. 4 presents a sketch of the shear frame geometry with applied loads and boundary conditions. Eq. 4.1 shows the relation between effective shear modulus and the shear rigidity. Q is the shear stiffness of the metal deck in the equation, G' is the effective shear modulus and s_d is tributary width of the deck. Calculation of tributary width of the deck is also given in equation 4.2. In this equation n_g is the number of the girders.

$$Q = G' s_d \tag{4.1}$$

$$s_d = \frac{n_g - 1}{n_g} \tag{4.2}$$

Through Equation 4.3 effective shear modulus of the system is obtained. This value is utilized in the equation 4.1 to calculate the shear rigidity of the diaphragm In Equation 4.3, P is the applied load, w is deck width, f is deck span and Δ is lateral displacement of the shear frame. The geometry of the model and the applied load were not changed. Merely, the area of the diagonal truss members could be altered until the target displacement achieved. The same geometry and diagonal truss areas were used in eigenvalue buckling and large deformation analyses.

$$G' = \frac{Pw}{\Delta f} \tag{4.3}$$

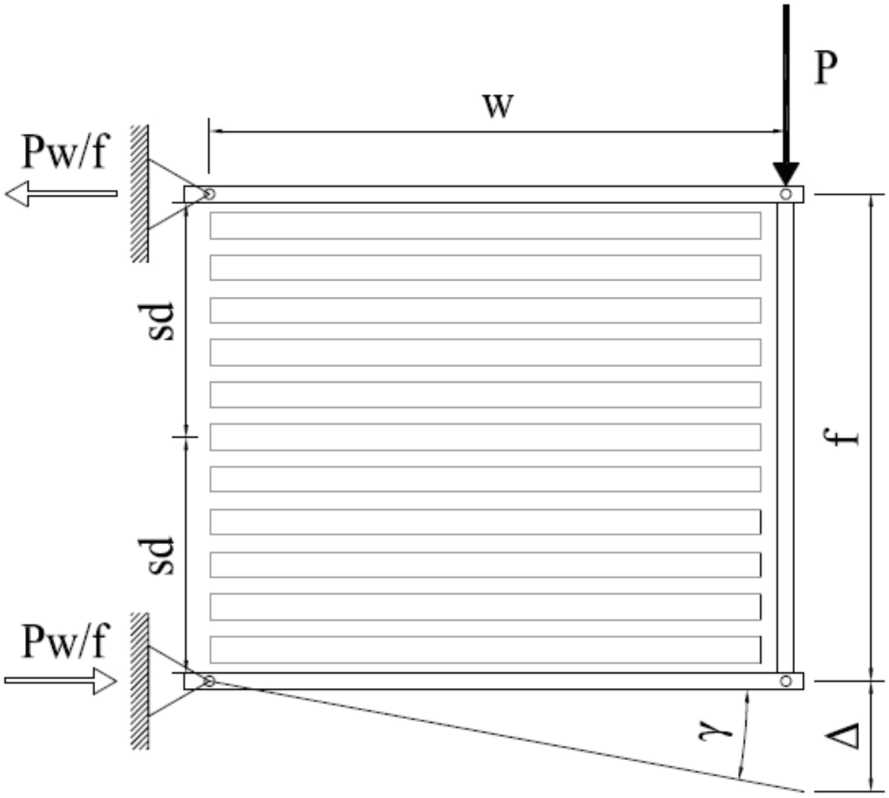

Figure 4. 4. Shear frame model used to determine the shear stiffness of decks.

The numerical analysis procedure used in the study is the large displacement analyses. In the numerical analysis, non-linear static analyses of imperfect twin girder system was conducted for the specified Q_i values by utilizing obtained diagonal truss areas. These areas controls the rigidity of the shear diaphragms. The loading procedure of large displacement analyses could be found under Section 3.2.

CHAPTER 5

FINITE ELEMENT RESULTS

5.1. Introduction

In this chapter, results from finite element analysis conducted on diaphragm braced twin-girder systems are presented. Non-linear large displacement analyses were conducted to obtain stiffness requirements of shear diaphragms. Results were grouped and presented as doubly symmetric stocky I-beams, doubly symmetric slender I-beams and singly symmetric slender I-beams. Consequently, the findings will be discussed briefly.

5.2. Doubly Symmetric I-Beams with Stocky Webs

L/d ratios of 15, 20, 25 and 30 were considered for stocky beams with a web slenderness ratio of 60. Results are presented in both tabular and graphical format. Figure 5. 1 illustrates the relation between normalized applied moment and mid-span twist ratios of two stocky beams with an *L/d* ratio of 30. Axis of the ordinate shows the normalized beam moment which is the applied moment at each load step divided by the maximum moment that corresponds to an in-plane bending moment of the section with a stress level of 210 MPa at the extreme fiber. On the horizontal axis, the mid-span resulting twist that is normalized by the initial twist is given. Thickness of the deck was 1.52 mm (16 ga) and number of the side lap fasteners along the seam were taken as five. Width of the deck was 610 mm and fastened to the top flange with four deck to structural edge fasteners. Results for two to five times (2, 3, 4 and 5) the ideal shear rigidity values are depicted. It could be examined from Figure 5. 1 that the normalized twists were measured as 4.02, 3.22, 2.89 and 4.51, 3.49, 3.11 for the diaphragms having rigidities of three to five times the ideal value, at the design load level for Stocky #1 and #2 sections, respectively. For both of the stocky beam sections, solution did not converge at the design load level for twice

the ideal rigidity value. Stocky #1 and #2 sections had normalized twist ratios of 6.87 and 5.96 at %94 and 90% of the design load levels, respectively.

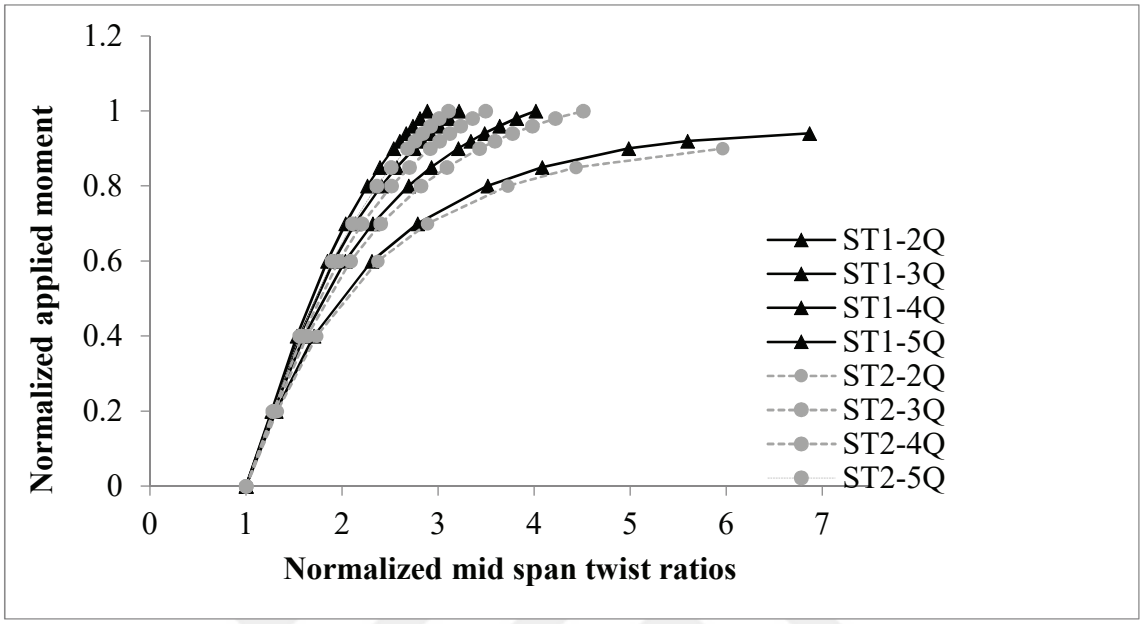

Figure 5. 1. Normalized applied moment versus normalized mid span twist ratios of Stocky#1 and Stocky#2 beams with an L/d ratio of 30.

Table 5.1 and Table 5.2 summarizes the results of finite element analysis on stocky sections. The table one is divided into eight columns labelled from (a) to (l). Columns from (a) to (c) demonstrate the name of the beam section, cross sectional properties, and *L/d* ratios, respectively. Columns from (d) to (g) indicate the normalized mid-span twist ratio for diaphragm shear rigidities of two to five times the ideal value at design load level. In Table 5.2, there are eleven columns. Columns from (h) to (o) indicate the respective edge and side lap fastener brace forces for diaphragms with shear rigidities of two to five times the ideal value while columns from (a) to (c) demonstrate the name of the beam section, cross sectional properties, and *L/d* ratios like in the first table. Deck thicknesses, edge fastener numbers and side-lap fastener numbers were same in all of the analysis and taken as 1.52 mm (16 ga), four and five respectively. As it could be observed from Table 5. 1, the total twists of Stocky #1 and #2 sections varied between 4.10 and 5.79 times the initial twists (L_b/500d) of the section for *L/d* ratios of 15, 20 and 25. The shear diaphragm rigidity have two times the ideal value in these cases. Increasing the shear rigidity of the diaphragms to three times the ideal value decreased the total twists

of the beams by about 30% to 40%. Further increasing the diaphragm rigidity to four times the ideal value decreased the total twists of the beams by approximately 15% to 23% with comparison to the twists of a diaphragm rigidity of three times the ideal value. Further increment of the diaphragm rigidity to five times the ideal value decreased the total twists of the beams by 9% to 11% with comparison to the twists of a diaphragm rigidity of four times the ideal value. As an example, for Stocky #2 beam with *L/d* ratio of 25, the maximum normalized mid-span twist ratios were 5.79, 3.38, 2.82, and 2.57 for shear diaphragms with rigidities of two to five times the ideal value, respectively. These reductions correspond to 41.6%, 16.6, and 8.9% in twists when the diaphragm rigidity was increased to three, four and five times the ideal value, respectively.

Table 5. 1 Normalized mid-span twist ratios of Stocky beams.

Section Designation (a)	Section Properties (b)	L/d (c)	θ_T/θ_o			
			$2Q_{ideal}$ (d)	$3Q_{ideal}$ (e)	$4Q_{ideal}$ (f)	$5Q_{ideal}$ (g)
Stocky#1 (SEC2)	b_f = 140 mm	15	4.29	2.84	2.37	2.15
	d = 366 mm	20	4.37	2.90	2.46	2.24
		25	5.39	3.25	2.73	2.48
	WSR = 60	30	X	4.02	3.22	2.89
Stocky#2 (SEC3)	b_f = 280 mm	15	4.10	2.77	2.34	2.13
	d = 732 mm	20	4.38	2.92	2.48	2.27
		25	5.79	3.38	2.82	2.57
	WSR = 60	30	X	4.51	3.49	3.11

Table 5. 2. Normalized brace forces of stocky beams

Section Designation (a)	Section Properties (b)	L/d (c)	$F_{br\text{-}edge}$ (N)				$F_{br\text{-}side}$ (N)			
			$2Q_{ideal}$ (h)	$3Q_{ideal}$ (i)	$4Q_{ideal}$ (j)	$5Q_{ideal}$ (k)	$2Q_{ideal}$ (l)	$3Q_{ideal}$ (m)	$4Q_{ideal}$ (n)	$5Q_{ideal}$ (o)
Stocky#1 (SEC2)	b_f = 140 mm	15	1971	1445	1281	1204	7704	5542	4832	4494
	d = 366 mm	20	2251	1598	1412	1327	8786	6184	5407	5069
		25	2927	1852	1601	1490	11489	7265	6251	5812
	WSR = 60	30	X	2360	1938	1768	X	9157	7502	6826
Stocky#2 (SEC3)	b_f = 280 mm	15	7739	5683	5019	4715	30345	22100	19531	18349
	d = 732 mm	20	9046	6408	5650	5303	35447	24972	21931	20545
		25	12425	7631	6575	6108	48761	29872	25681	23857
	WSR = 60	30	X	10296	8199	7420	X	40212	32000	28959

Previous studies show that the necessary brace stiffness for a specific beam section should be sufficiently large enough to control brace forces. Thus, the maximum brace forces that develop along the length of the beams and side lap regions need to be identified. Brace forces that develop in a single deck sheet are presented in Figure 5. 2

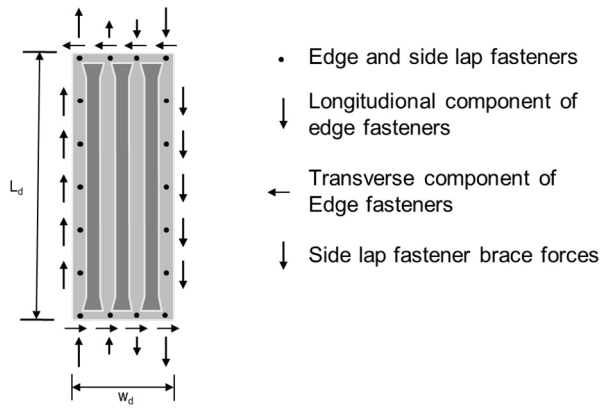

Figure 5. 2. Brace forces that develop in a single deck sheet.
(Source: Egilmez et al., 2014)

The standard single deck configuration utilized in this study has three corrugations, four edge fasteners, and five side lap fasteners. As presented in Figure 5. 2 both transverse and longitudinal forces develop at edge fasteners; while only transverse shear forces develop at side lap fasteners.

Considering the Stocky #1 and #2 beams with *L/d* ratio of 25, a diaphragm rigidity of four times the ideal value, five side lap fasteners along the seams and deck thickness of 1.52 mm (16 ga), the distribution of the resultant forces developed in edge fasteners along the beam top flange is presented in Figure 5. 3.

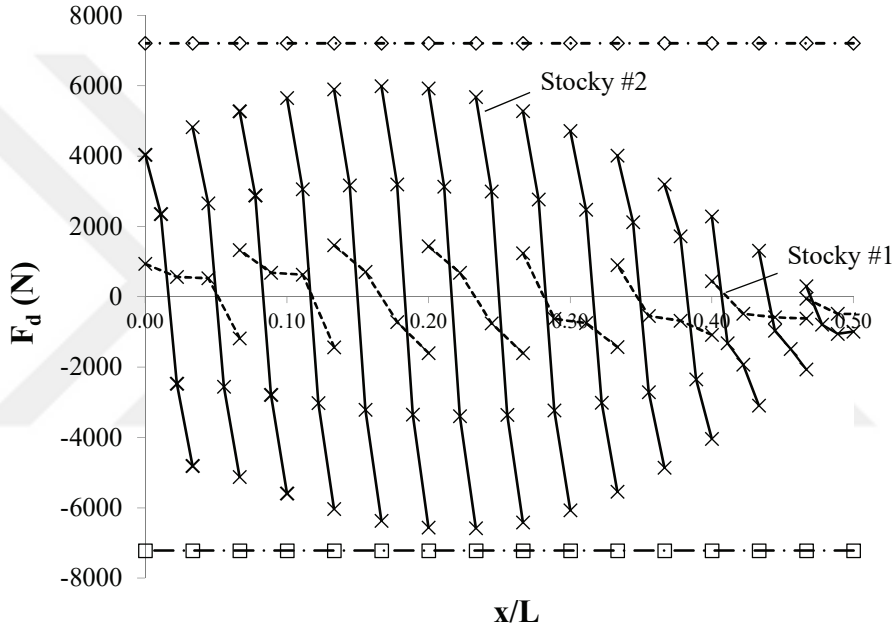

Figure 5. 3. Resultant end fastener brace forces of Stocky#1 and Stocky#2 beams with L/d ratio of 25 and Q=4Qi.

The resultant forces are calculated by taking vectorial resultant of the transverse and longitudinal force components that develop in each edge fastener. Due to symmetry with respect to midspan, brace forces are shown for half of the span. There are a total of nine and eighteen deck sheets along half of the beam lengths in Stocky #1 and Stocky#2 sections, respectively. Each dashed line drawn in the figure belongs to a single deck sheet. Also, the data markers on the lines represents the forces in the fasteners along the edge of a single sheet. It can be seen in Figure 5. 3 that maximum fastener forces develop around quarter span for both of the beams, where shear deformations are maximum. The

maximum brace forces that develop in Stocky #2 sections were approximately four times higher than the forces that develop in Stocky #1 sections.

The horizontal lines to the top and bottom of the vertical axis in Figure 5. 3 specify the amount of the maximum fastener brace force (7213 N) calculated by Eq. 2.25 for Stocky #1 section. This suggested value from previous work (7213 N) is approximately 4.50 times higher than the maximum resultant fastener force calculated by the analysis results. The force at the edge fastener for Stocky #2 beam (28855 N) calculated by Eq. 2.25 is not depicted in the figure, due to being beyond the graph limits. For Stocky #2 beam the calculated value of edge fastener force from Eq. 2.25 was 4.39 times higher than the maximum value measured from the analysis. The main reason for this difference of edge fastener forces is that, Helwig and Yura's study ignores the effects of side lap fasteners and the equation is derived for a stress level of 345 MPa which corresponds to the tensile yield strength of the steel material. This stress level is approximately 64% higher than the stress level used in this study (210 MPa).

Figure 5. 4 illustrates the side lap force distribution along half of the beam length for Stocky #1 and #2 sections of a shear diaphragm with a rigidity of four times the ideal value. There are five side lap fasteners along the seams and the deck thickness is 1.52 mm (16 ga). Analysis results are presented for L/d ratios of 15, 20, 25, and 30. As stated before, side lap fasteners were modeled utilizing transverse uniaxial tension-compression truss elements (LINK8). The stiffness of the transverse truss elements symbolizes the total stiffness of the fasteners connecting the decks together on overlapping region. The data markers in Figure 5. 4 represent the brace force in a side lap fastener at each seam. The force in a single side lap fastener is the average force per fastener along that lap. It was presumed that the side lap fastener force develops at a seam was split evenly by the side lap fasteners along the seam. The observed distribution of forces in Figure 5. 4 are similar to the edge fastener force distribution along the beam. The maximum side lap fastener forces also developed around quarter length of the beam. The brace forces that are measured in Stocky #2 beam were nearly 3 to 5 times higher than the forces that occurred in Stocky #1 beams. It is seen from the figure that increasing the L/d ratios resulted in an increment in side lap brace forces. The rise in brace forces were more substantial in Stocky #2 beams, with comparison to the change in force levels observed in Stocky #1 beams for variable L/d ratios.

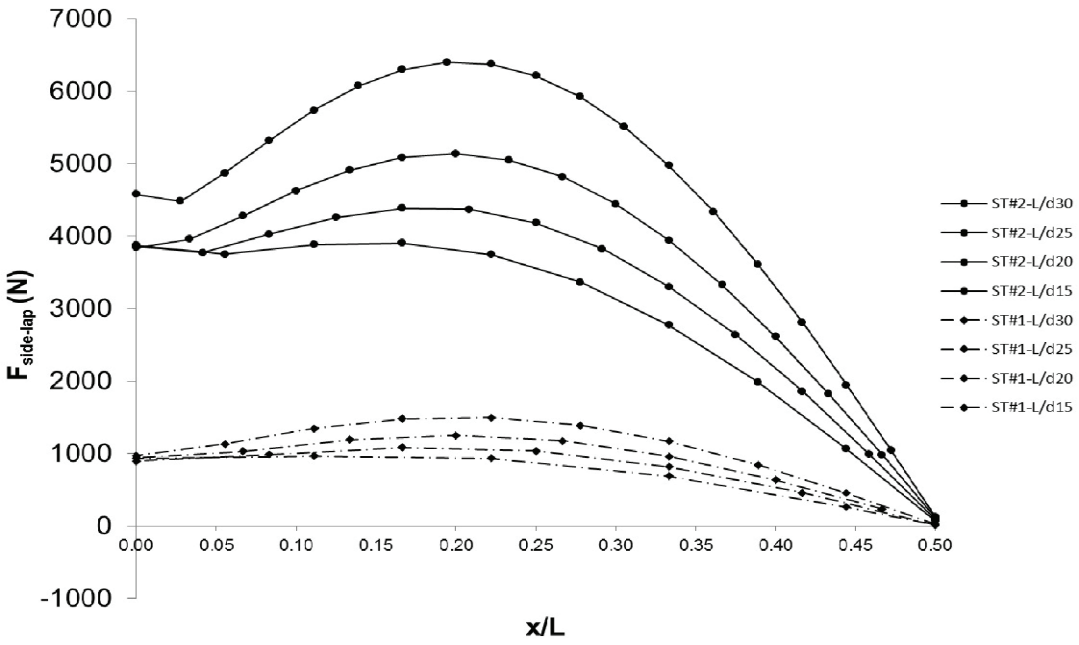

Figure 5. 4. Sidelap fastener forces along the beam for Stocky#1 and Stocky#2 beams with diaphragm rigidity of four times the ideal value and L/d ratios of 15, 20, 25 and 30.

The maximum edge and side lap fastener brace forces ($F_{br\text{-}e}$ and $F_{br\text{-}sl}$), that develop at the design load level, along the length of the beams with stocky sections are tabulated from columns (h) to (o) in Table 5.2. As it can be observed from the table, using a section with a deeper web increases the fastener forces to higher values than the value of the increment in maximum twist. For instance, for an *L/d* ratio of 25 and a diaphragm rigidity of three times the ideal value, the mid-span normalized twist of Stocky #2 section was 4.0% higher than that of Stocky #1 section (3.38 vs. 3.25 for Stocky #2 and #1 sections, respectively). Conversely, for the same *L/d* ratio and shear diaphragm rigidity, the maximum edge and side lap fastener brace forces that occur in Stocky #2 beam were nearly four times higher than the respective values of Stocky #1 beam. Similar behavior was observed for various *L/d* ratios and diaphragm rigidities. The extraordinary rise in fastener brace forces is possibly because of the increase in load levels between Stocky #1 and #2 beams with the same span/depth ratios. Although the web slenderness ratio and the stress levels were the same for the two sections, Stocky #2 beams carry about four times more load than the Stocky #1 beams.

It could also be seen in Table 5.2 that for both sections, increasing the diaphragm rigidity from twice and three times the ideal value decreased the maximum edge and side lap fastener brace forces by 27% to 39% respectively. Further increment of the diaphragm rigidity to four times the ideal value decreased the fastener brace forces by an extra 11% to 20%. Further increment of the diaphragm rigidity to five times, the fastener forces dropped by an extra 6% to 10%. For instance, for Stocky #2 beam with an *L/d* ratio of 20, the respective maximum edge fastener forces ($F_{br\text{-}e}$) were 9046 N, 6408 N, 5650 N, and 5303 N for a shear diaphragm with rigidities of two to five times the ideal value. For the same section, the maximum side lap fastener brace forces ($F_{br\text{-}sl}$) were 35447 N, 24972 N, 21931 N, and 20545 N for a shear diaphragm with rigidities of two to five times the ideal value.

5.3. Doubly and Singly Symmetric I-Beams with Slender Web

The beams that were discussed in the previous section had stocky webs, which are commonly utilized in building industry. Results discussed in this section will concentrate on the sections with deeper webs, both doubly and singly symmetric. The width to span ratios (WSRs) of 100 and 160 that are widely used in plate girders, will be considered. The relatively slender webs of the beams resulted higher risk of web shear buckling. Nevertheless, since the assumed stress level (210 MPa) in this study is comparatively low, web shear buckling was not observed in the analyses. Four doubly symmetric slender sections (with depths of 1464 mm and 1830 mm) and six singly symmetric slender sections (with a depth of 1464 mm) were studied. The *L/d* ratios of 20, 25, and 30 that were used in the previous section are not used for the selected cross sections. For such *L/d* ratios the bending moment due to self-weight of the beams either surpassed or was extremely close to the lateral torsional buckling capacity of the sections. The deck systems used in all of the analyses had 1.52 mm (16 ga) thickness of deck sheet. There are four edge fasteners, and five side lap fasteners along the seams.

The normalized mid-span twist ratio and edge/side lap fastener brace forces for the members defined are listed in Table 5.3, Table 5.4 Table 5.5 and Table 5.6 respectively. These tables have the same format with Table 5.1 and Table 5.2. It can be noted for Table 5. 3 that for a shear diaphragm with rigidity of twice the ideal value, the ratio of total mid-span twist ratios to the initial twists (θ_T/θ_o) of doubly symmetric beams

varies between 3.57 for Slender-100 #1 beam and 4.74 for Slender-160 #2 beam. Increasing the diaphragm rigidity to three, four, and five times the ideal value decreased the twists by approximately 28.3%, 13.0%, and 7.0%, with comparison to the twists observed on the beams with diaphragm rigidities of two, three, and four times the ideal value, respectively. For instance, for the most slender doubly symmetric section, Section-160 #2, with a *L/d* ratio of 15 and WSR of 160, the respective ratios of total twist to initial twist were observed as 4.74, 3.30, 2.87, and 2.66 for a shear diaphragm with rigidities of two to five times the ideal value. These values correspond to reductions of 30% (from two times the ideal rigidity to three times), 13% (from three times the ideal rigidity to four times), and 7% (from four times the ideal rigidity to five times) in mid-span twist.

Table 5. 3. Normalized mid-span twist ratios of doubly symmetric slender I-beams.

Section Designation (a)	Section Properties (b)	L/d (c)	θ_T/θ_o			
			$2Q_{ideal}$ (d)	$3Q_{ideal}$ (e)	$4Q_{ideal}$ (f)	$5Q_{ideal}$ (g)
Slender-100#1	b_f = 300 mm	10	3.57	2.57	2.24	2.08
	d = 1464 mm	15	3.99	2.87	2.50	2.33
Slender-160#1	b_f = 300 mm	10	3.83	2.72	2.36	2.18
	d = 1464 mm	15	4.22	2.98	2.59	2.40
Slender-100#2	b_f = 300 mm	10	3.74	2.73	2.39	2.22
	d = 1464 mm	15	4.38	3.13	2.74	2.55
Slender-160#2	b_f = 300 mm	10	3.96	2.88	2.52	2.34
	d = 1464 mm	15	4.74	3.30	2.87	2.66

Table 5. 4. Normalized brace forces of doubly symmetric slender I-beams.

Section Designation (a)	Section Properties (b)	L/d (c)	$F_{br\text{-}edge}$ (N)				$F_{br\text{-}side}$ (N)			
			$2Q_{ideal}$ (h)	$3Q_{ideal}$ (i)	$4Q_{ideal}$ (j)	$5Q_{ideal}$ (k)	$2Q_{ideal}$ (l)	$3Q_{ideal}$ (m)	$4Q_{ideal}$ (n)	$5Q_{ideal}$ (o)
Slender-100#1	b_f = 300 mm	10	13110	9989	8990	8549	10225	7758	6981	6618
	d = 1464 mm	15	15857	11861	10613	9989	12354	9212	8238	7779
Slender-160#1	b_f = 300 mm	10	12486	9364	8365	7991	9759	7319	6549	6191
	d = 1464 mm	15	14608	10738	9614	8990	11476	8407	7475	7042
Slender-100#2	b_f = 300 mm	10	17405	13222	11899	11275	13591	10306	9266	8772
	d = 1464 mm	15	21725	15982	14234	13344	17011	12483	11090	10424
Slender-160#2	b_f = 300 mm	10	15520	11724	10525	9976	12124	9151	8205	7772
	d = 1464 mm	15	19603	13984	12361	11612	15348	10969	9705	9117

Table 5. 5. Normalized mid-span twist ratios of singly symmetric slender I-beams.

Section Designation (a)	Section Properties (b)	L/d (c)	θ_T/θ_o			
			$2Q_{ideal}$ (d)	$3Q_{ideal}$ (e)	$4Q_{ideal}$ (f)	$5Q_{ideal}$ (g)
SS-100# 19	b_{cf} = 210 mm I_{yc}/I_y = 0.19 d = 1464 mm WSR = 100	10	3.24	2.34	2.05	1.90
		15	3.73	2.66	2.32	2.16
SS-100# 29	b_{cf} = 240 mm I_{yc}/I_y = 0.29 d = 1464 mm WSR = 100	10	3.33	2.41	2.10	1.95
		15	3.84	2.73	2.38	2.21
SS-100# 39	b_{cf} = 270 mm I_{yc}/I_y = 0.39 d = 1464 mm WSR = 100	10	3.49	2.50	2.18	2.02
		15	3.96	2.81	2.45	2.28
SS-160# 19	b_{cf} = 210 mm I_{yc}/I_y = 0.19 d = 1464 mm WSR = 160	10	3.51	2.46	2.13	1.97
		15	4.02	2.77	2.39	2.21
SS-160# 29	b_{cf} = 240 mm I_{yc}/I_y = 0.29 d = 1464 mm WSR = 160	10	3.57	2.52	2.19	2.03
		15	4.01	2.81	2.44	2.26
SS-160# 39	b_{cf} = 270 mm I_{yc}/I_y = 0.39 d = 1464 mm WSR = 160	10	3.66	2.61	2.26	2.10
		15	4.16	2.91	2.52	2.34

Table 5. 6. Normalized brace forces of singly symmetric slender I-beams.

Section Designation (a)	Section Properties (b)	L/d (c)	$F_{br\text{-}edge}$ (N)				$F_{br\text{-}side}$ (N)			
			$2Q_{ideal}$ (h)	$3Q_{ideal}$ (i)	$4Q_{ideal}$ (j)	$5Q_{ideal}$ (k)	$2Q_{ideal}$ (l)	$3Q_{ideal}$ (m)	$4Q_{ideal}$ (n)	$5Q_{ideal}$ (o)
SS-100# 19	b_{cf} = 210 mm I_{yc}/I_y = 0.19 d = 1464 mm WSR = 100	10	9701	7254	6493	6143	7576	5657	5055	4771
		15	11512	8390	7441	6992	8982	6535	5792	5447
SS-100# 29	b_{cf} = 240 mm I_{yc}/I_y = 0.29 d = 1464 mm WSR = 100	10	10675	8066	7229	6842	8319	6265	5616	5312
		15	12848	9427	8365	7878	10016	7346	6522	6137
SS-100# 39	b_{cf} = 270 mm I_{yc}/I_y = 0.39 d = 1464 mm WSR = 100	10	11974	9027	8103	7666	9320	7002	6278	5941
		15	14409	10600	9427	8877	11246	8259	7353	6920
SS-160# 19	b_{cf} = 210 mm I_{yc}/I_y = 0.19 d = 1464 mm WSR = 160	10	8852	6430	5693	5356	6914	5021	4454	4190
		15	10376	7279	6393	5981	8076	5697	5001	4683
SS-160# 29	b_{cf} = 240 mm I_{yc}/I_y = 0.29 d = 1464 mm WSR = 160	10	9801	7229	6443	6068	7657	5636	5015	4731
		15	11325	8178	7242	6792	8880	6407	5663	5319
SS-160# 39	b_{cf} = 270 mm I_{yc}/I_y = 0.39 d = 1464 mm WSR = 160	10	10925	8178	7317	6917	8563	6380	5704	5386
		15	12985	9402	8328	7829	10171	7353	6515	6116

For singly symmetric slender beams, the ratio of total mid-span twist ratio to initial twist (θ_T/θ_o) varies between 3.24 for SS-100 #19 section with an L/d ratio of 10 and 4.16 for SS-160 #39 section with an L/d ratio of 15 in Table 5. 5. The amount of these reductions in θ_T/θ_o for all of the singly symmetric beams were identical to the reductions obtained in doubly symmetric beams when the diaphragm rigidities were increased to three, four, and five times the ideal value from two, three, and four times the ideal value, respectively. For instance, for SS-100 #29 section with a depth of 1464 mm, WSR of 100, L/d ratio of 10, and I_{yc}/I_y = 0.29, the respective ratios of total twist to initial twist were 3.33, 2.41, 2.10, and 1.95 for diaphragm rigidities of two, three, four, and five times

the ideal value. These values correspond to reductions of 28%, 13%, and 7% in mid-span twist ratios when the diaphragm rigidities were increased to three, four, and five times the ideal value from two, three, and four times the ideal value, respectively.

Analogous with the drop in twists, increasing the diaphragm rigidity to three, four, and five times the ideal value similarly decreased the edge and side lap fastener brace forces in both doubly and singly symmetric beams. For doubly symmetric beams the respective drops in both end and side lap fastener brace forces were approximately 25.6%, 10.8%, and 5.5% when the diaphragm rigidities were dropped to three, four, and five times the ideal value from two, three, and four times the ideal value; as can be examined in Table 5.2. For instance, for Slender-160 #1 section with a span/depth ratio of 15, WSR of 10, and deck thickness of 1.52 mm (16 ga) the maximum edge fastener brace forces were 12486 N, 9364 N, 8365 N, and 7991 N for diaphragm rigidities of two, three, four, and five times the ideal value. Side lap fastener brace forces were measured as 9759 N, 7319 N, 6549 N, and 6191 N correspondingly. These values correspond to percent reductions of approximately 25%, 11%, and 5% for both maximum edge and side lap fastener brace forces when the diaphragm rigidity is increased to three, four, and five times the ideal value from two, three, and four times the ideal value, respectively.

The effects of web slenderness ratio and beam depth on mid-span twist ratios and brace forces can be found in Table 5. 4 and Table 5. 5 as well. In order to observe the effects of web slenderness ratio, normalized twists and brace forces of Slender-100 #1 (beam depth = 1464 mm, WSR = 100) and Selnder-160 #1 (beam depth = 1464 mm, WSR = 160) beams can be compared. For a shear diaphragm with a rigidity of three times the ideal value and *L/d* ratio of 15, for instance, the respective values of normalized mid-span twist ratio, maximum edge fastener force, and maximum side lap fastener force were 2.87, 11861 N, and 9212 N for Slender-100 #1 beam. When the web slenderness ratio was increased to 160 (Slender-160 #1), normalized mid-span twist ratio increased to 2.98 (3.8% increase), maximum edge fastener force decreased to 10738 N (9.5% decrease), and maximum side lap fastener force decreased to 8407 N (8.8% decrease). A diverse behavior was noted when web slenderness ratio was kept constant and depth of the beam was increased. With comparison of the normalized mid-span twist ratios and brace forces of Slender-100 #1, which has a beam depth of 1464 mm and WSR of 100, and Slender-100 #2, which as a beam depth of 1830 mm and WSR of 100, sections disclose that not only the normalized twists but also fastener brace forces increased when a deeper beam was used. For the specific rigidity value of the diaphragm and *L/d* ratio the respective

normalized mid-span twist ratio, maximum edge fastener force, and maximum side lap fastener force were 3.13, 15982 N, and 12483 N for Slender-100 #2 section. These values signify an increase of approximately 9.1%, 34.7%, and 35.5% in mid-span twist ratio, maximum edge fastener force, and maximum side lap fastener force, respectively. The increase in brace forces due to an increase in depth of the beam is more probably owing to the higher uniform distributed load demanded to develop a stress level of 210 MPa (30.43 ksi) at the extreme fiber of the sections with higher depths with comparison to those of the beams with smaller web depths.

For singly-symmetric slender beams maximum edge and side lap fastener forces are listed in Table 5. 6. As it observed in Table 5. 6 six singly symmetric sections with a depth of 1464 mm, WSR of 100 and 160, and mono-symmetry (I_{yc}/I_y) ratios of 0.19, 0.29, and 0.39 were studied. The reductions in maximum edge and side lap fastener forces in singly symmetric beams were similar percentage to those seen in doubly symmetric slender beams. Increment in the shear rigidity of the diaphragm to three, four, and five times the ideal value decreased both the edge and side lap fastener forces in entire six sections by nearly 26.5%, 10.8%, and 5.8% with respect to the forces measured in systems with a diaphragm with rigidities of two, three, and four times the ideal value, respectively. A parallel behavior was noticed in the effect of web slenderness ratio on normalized mid-span twist ratio as well as maximum edge and side lap fastener forces. Table 5. 5 and Table 5. 6 clarifies that normalized mid-span twist ratios increased and maximum edge and side lap fastener forces dropped when the web slenderness ratio of the beams increased. For instance, for a shear diaphragm with rigidity of four times the ideal value, normalized mid-span twist ratio, maximum edge fastener force, and maximum side lap fastener force were 2.10, 7229 N, and 5616 N correspondingly for SS-100 #29 beam with a web slenderness ratio of 100 and *L/d* ratio of 10. With the increment in web slenderness ratio to 160 (SS-160 #29), normalized mid-span twist ratio increased to 2.19 (4.3% increment), maximum edge fastener force dropped to 6443 N (10.9% decrease), and maximum side lap fastener force dropped to 5015 N (10.7% decrease). A similar performance was noted in other singly symmetric beams.

Figure 5. 5 and Figure 5. 6 depicts the normalized applied moment versus maximum edge and side lap fastener forces for doubly symmetric Slender-100 #1 and singly symmetric SS-100 #39, #29, and #19 sections for a shear diaphragm with rigidity of four times the ideal value and *L/d* ratio of 15. It is observed in Figure 5. 5 and Figure 5. 6 that at the design load level the maximum edge fastener force ($F_{br\text{-}e}$) was 10613 N

for doubly symmetric Slender-100 #1 section that has a mono-symmetry ratio of 0.50. At this load level, the maximum edge fastener forces of singly symmetric SS-100 #39, #29, and #19 beams (with respective ratios of mono-symmetries of 0.39, 0.29, and 0.19) decreased to 9427 N, 8365 N, and 7441 N, respectively. The maximum side lap fastener force ($F_{br\text{-}sl}$) at the design load was 8238 N for doubly symmetric Slender-100 #1 section. As the ratio of mono-symmetry (I_{yc}/I_y) decreased to 0.39, 0.29, and 0.19 the maximum side lap fastener forces dropped to 7353 N, 6522 N, and 5792 N for singly symmetric SS-100 #39, #29, and #19 sections, respectively. The reduction in maximum edge and side lap fastener forces was nearly 11% for each drop in mono-symmetry (for example from I_{yc}/I_y = 0.5 to I_{yc}/I_y = 0.39, from I_{yc}/I_y = 0.39 to I_{yc}/I_y = 0.29, and from I_{yc}/I_y = 0.29 to I_{yc}/I_y = 0.19). The effect of mono-symmetry on normalized mid-span twist ratio was less crucial. For instance, Table 5. 3 and Table 5. 5. explains that, for a shear diaphragm with rigidity of four times the ideal value and an *L/d* ratio of 15, the respective normalized mid-span twist ratios of doubly symmetric Slender-100 #1 and singly symmetric SS-100 #39, #29, and #19 beams were 2.50, 2.45, 2.38, and 2.32. These reductions were 2.0%, 2.9%, and 2.5% correspondingly. Similar behaviors were observed in other singly-symmetric sections.

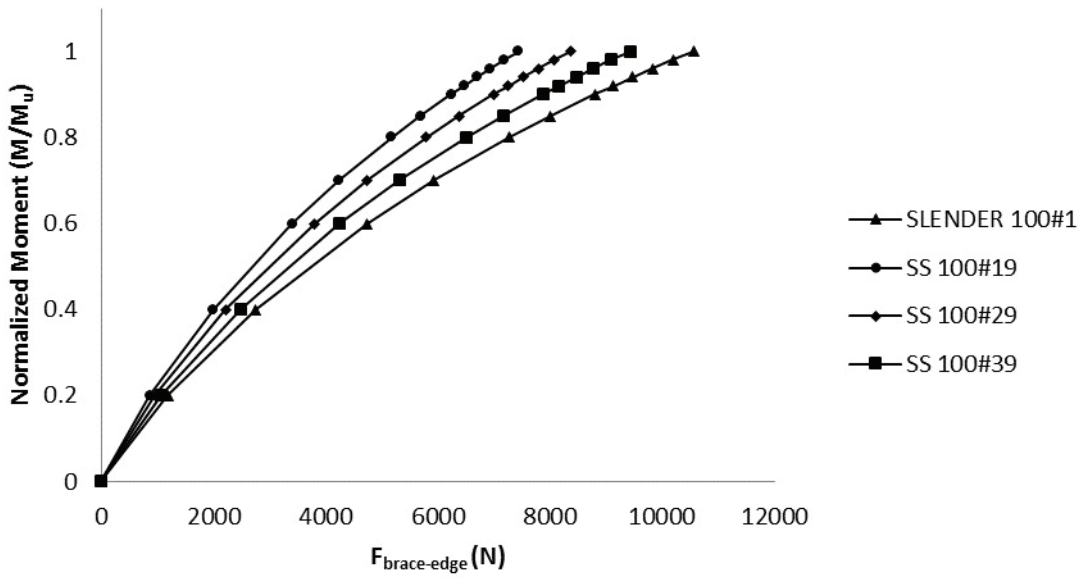

Figure 5. 5. Normalized applied moment versus maximum edge fastener forces for Slender 100#1,SS-100#39, #29, #19 beams with an L/d ratio of 15

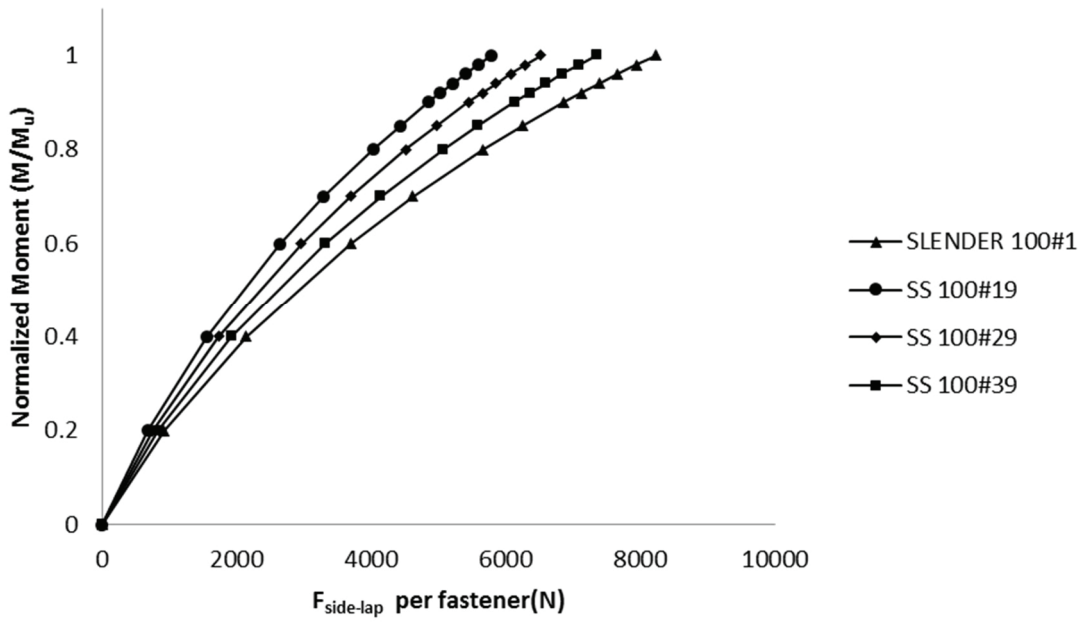

Figure 5. 6. Normalized applied moment versus maximum side lap fastener forces (per fastener) for Slender 100#1,SS-100#39, #29, #19 beams with an L/d of 15

5.4. Diaphragm Stiffness Requirements of I-Beams

In this study the behavior of steel I-beams braced by metal deck forms continuously at the compression flange was examined to develop stiffness requirements of the shear diaphragms. Six doubly symmetric and six singly symmetric sections with WSR of 60, 100, and 160, *L/d* ratios of 10, 15, 20, 25, and 30, and web depths of 366 mm (14.4 in), 732 mm (28.8 in), 1464 mm (57.6 mm), and 1830 mm (72 in) were used. Only top flange distributed loading case was considered. The design load level for the sections was chosen as the bending moment corresponding to an in-plane stress equal to 210 MPa (30.4 ksi) at the extreme fiber of the beam sections.

The results reveals that providing twice the ideal rigidity results in relatively large normalized mid-span twist ratios at the maximum design load for the entire sections utilized. Stocky beams with *L/d* ratio of 30 did not converge and could only reach 90% of the design load level. Increasing the diaphragm rigidity to three times the ideal value, which means a 50% increment in the rigidity of the diaphragm, decreased the normalized mid-span twist ratio values approximately 35.8%, 28.3%, and 30.0% for stocky, doubly symmetric slender, and singly symmetric slender beams, respectively. Further increasing the diaphragm rigidity to four times the ideal value, a 33.3% increase in the rigidity of a

diaphragm, decreased the mid-span twist ratios approximately 17.1% and 12.9% for stocky and slender beams. Providing a shear diaphragm with a rigidity of four times the ideal value limits the normalized mid-span twist ratios of entire sections below three, except for stocky beams with *L/d* ratio of 30. Increasing the diaphragm rigidity to five times the ideal value further dropped the twists approximately 9.5% and 7.1% for stocky and slender sections, respectively. Nevertheless, the reductions are not significant enough when compared to the 25% increment in brace stiffness.

Similar percent reductions were examined in brace forces for increasing the rigidity of diaphragms. Providing a diaphragm rigidity of three times the ideal value instead of two reduces both the edge and side lap fastener brace forces approximately 31% and 25% for stocky and slender beams, respectively. Increasing the diaphragm rigidity to four times the ideal value, a 33.3% increase in the rigidity of the diaphragm, drops the edge and side lap fastener brace forces by nearly 14% and 16%, respectively. For slender beams the reductions in both edge and side lap fastener brace forces were nearly 10.8%. Further increasing the diaphragm rigidity to five times the ideal value, a 25% increase in the rigidity of the diaphragm, dropped the edge and side lap fastener brace forces by nearly 7% and 5.5% for stocky and slender beams, respectively. The reductions in brace forces provided by increasing the rigidity of the diaphragm to five times the ideal value are not significant enough as well when compared to the 25% increment in brace stiffness.

Based on the observations discussed above, a shear diaphragm stiffness equal to four times the ideal value will be suggested to limit deformations and brace forces for shear diaphragms in order to brace steel I-beams. Equation 2.21, which was suggested by Helwig and Frank (1999) to calculate the buckling capacity of diaphragm braced beams, can be used to resolve for the required effective diaphragm shear stiffness as given below:

$$G'_{req'd} = \frac{4(M_u - C_b^* M_g)}{mds_d} \tag{5.1}$$

The equation given above is valid for the sections analyzed in this study. These sections are: (a) Stocky sections with WSR of up to 60, depth of up to 732 mm (28.8 in), and *L/d* ratio of up to 30; (b) Doubly symmetric sections with WSR of up to 160, depth of 1830 mm (72 in), and *L/d* ratio of up to 15; and (c) Singly symmetric sections with WSR of up to 160, depth of up to 1464 mm (57.6 in), and *L/d* ratio of up to 15. The design

stress level utilized to derive Eq. (11) was 210 MPa (30.4 ksi). For stress levels higher than 210 MPa (30.4 ksi) the required effective shear stiffness can also be taken as four times the ideal value as recommended by Helwig and Yura (2008b).

Designers can utilize the equations and the design tables involved in the SDI Manual (Luthrell, 2004) or test results from previous works (such as Egilmez et al. 2007) to choose the proper deck layout that will meet the stiffness demands suggested by Eq. (5.1). Proper factors should also be applied to Eq. (5.1) such as Φ=0.75 in load and resistance factor design (LRFD) and Ω=2.0 in allowable stress design (ASD).

CHAPTER 6

CONCLUSIONS

6.1. Summary and Conclusions

Stability requirements of steel I-beams braced by shear diaphragms are investigated. In order to conduct the numerical studies on the lateral torsional buckling behavior of the twin steel I-beam systems, a three dimensional analysis programme (ANSYS Mechanical APDL, 2007) is utilized. Numerical studies were performed on both perfectly straight and initially imperfect twin girder-deck system models. Value of the applied initial imperfection was $L_b/500d$ which has a sinusoidal path and with zero values at the supports. In this imperfection pattern, bottom flange remained straight as the top flange displaced laterally through the beam section. In the study, material nonlinearity was not modelled, therefore all the finite elements have linearly elastic material properties. Both doubly and singly-symmetric sections with various parameters were studied. For both type of these sections, web slenderness ratio were taken 58 for stocky sections and 100 and 160 for slender sections. Similarly, flange slenderness ratios were 7.78 for stocky beams and 6 for all slender sections. Span to web depth was also limited for the sections. For stocky beams L/d ratios of 15, 20, 25 and 30 were investigated. This ratios were kept 10 and 15 for slender beams due to disadvantages of the cross sectional properties. A value of 210 MPa is designated for the target stress level at the outer fiber. This stress level is generally reached after the erection of steel I-beams. The distributed loading to create the moment value that results the intended stress level was applied at the top flange of the beams. The finite element mathematical model was verified by utilizing the results of a full-scale twin-girder diaphragm buckling test (Egilmez et al., 2005). Upon obtaining the ideal shear rigidities, shear frame analyses were performed to obtain the areas of diagonal truss members that signify the diaphragm rigidities. After that, large displacement analyses were performed on initially imperfect girders with specified stiffness values of diaphragm configurations. The analysis results are evaluated to examine the mid-span twists and brace forces developing on the edge and side lap

fasteners. Brace forces and rotations were normalized to develop generalizations that is free of the specific member sizes.

According to rotation results, the findings are as follows;

- Increasing the span to depth ratios causes higher mid-span twist ratios,
- Providing a deck with higher stiffness reduces the mid-span twist ratios of the section,
- Center of twist of the sections are moving upwards as the deck stiffness increases,
- As the center of twist gets closer to the compression flange, increasing the deck stiffness loses its effectiveness,
- For the same slenderness ratio and span to depth ratio, beams with smaller aspect ratio in cross section has smaller mid-span twists,
- For singly-symmetric slender sections, beams with smaller mono-symmetry ratios have smaller mid-span twist ratios.

According to the bracing force results, the findings are as follows;

- Along the length of the section maximum bracing forces develop around quarter span, where the shear deformations are maximum,
- Higher bracing forces occur in the sections that are subjected to higher flexural moments and higher compression forces (it should be noted that higher internals forces develop in the sections with larger moment of inertias),
- Increasing the span to depth ratio resulted in higher bracing forces,
- Maximum bracing force of the edge fasteners in a single deck generated at the first and the last fasteners,
- The side-lap fastener forces are higher than the edge fasteners and the demand of the side-lap connections is smaller than that of the edge fastener connections.

In conclusion, based on the observations given above, singly symmetric sections with smaller mono-symmetry ratios provide a better rotational behavior and a shear diaphragm stiffness equal to four times the ideal value will be suggested to limit deformations and brace forces for shear diaphragms in order to brace steel I-beams.

REFERENCES

American Association of State Highway and Transportation Officials. (2012). *AASHTO LRFD bridge design specifications, customary U.S. units*. Washington, DC: American Association of State Highway and Transportation Officials.

American Institute of Steel Construction. (2001). *Load and resistance factor design specification for structural steel buildings*. Chicago, Ill: American Institute of Steel Construction.

American Institute of Steel Construction. (2005). *Specification for structural steel buildings*. Chicago, Ill: American Institute of Steel Construction.

American Institute of Steel Construction. (2010). *Specification for structural steel buildings*. Chicago, Ill: American Institute of Steel Construction.

ANSYS Inc. (2011). Elements Reference. *Release 14.0 Documentation for ANSYS.*

Cordeck Building Solutions (2014). Floor Decks. Retrieved December 28, 2014, from http://www.cordeck.com/metal-deck-products/form-deck

Davies, J. M., & Bryan, E. R. (1982). *Manual of stressed skin diaphragm design*. London: Granada.

Egilmez, O. Ö. (2005). *Lateral Bracing of Steel Bridge Girders by Permanent Metal Deck Forms.* Ph.D. Dissertation Department of Civil and Environmental Engineering; State University of Houston.

Egilmez, O. Ö., Helwig, T. A., Jetann, C. A., & Lowery, R. (2007). Stiffness and strength of metal bridge deck forms. *Journal of Bridge Engineering*, *12*(4), 429-437.

Egilmez, O. Ö., Helwig, T. A., & Herman, R. (2009). Lateral stiffness of steel bridge I-girders braced by metal deck forms. *Journal of Bridge Engineering*, *14*(1), 17-25.

Egilmez, O. Ö., Helwig, T. A., & Herman, R. (2012). Buckling behavior of steel bridge I-girders braced by permanent metal deck forms. *Journal of Bridge Engineering*, *17*(4), 624-633

Egilmez, O. Ö., Akbaba, A., & Vardaroglu, M. (2014). Stiffness and strength of shear diaphragms used for stability bracing of slender beams. *Proceedings of the Annual Stability Conference Structural Stability Research Council,* Toronto.

Errera, S., & Apparao, T. (1976) Design of I-shaped beams with diaphragm bracing. *J. Struct. Div.*, ASCE, 102(4), 769–781.

Galambos, T. V. (1998). *Guide to stability design criteria for metal structures*. New York: John Wiley.

Helwig, T. A. (1994). *Lateral Bracing of Bridge Girders by Metal Deck Forms.* Ph.D. Dissertation Faculty of the Graduate School; State University of Texas.

Helwig, T. A., Frank, K. H., & Yura, J. A. (1997). Lateral-torsional buckling of singly symmetric I-beams. *Journal of Structural Engineering*, *123*(9), 1172-1179.

Helwig, T. A., & Frank, K. H. (1999). Stiffness requirements for diaphragm bracing of beams. *Journal of Structural Engineering*, *125*(11), 1249-1256.

Helwig, T. A., & Yura, J. A. (2008). Shear diaphragm bracing of beams. I: Stiffness and strength behavior. *Journal of Structural Engineering*, *134*(3), 348-356.

Helwig, T. A., & Yura, J. A. (2008). Shear diaphragm bracing of beams. II: Design requirements. *Journal of Structural Engineering*, *134*(3), 357-363.

Helwig, T. A. (2013). *2013 NASCC presentations: Steel Bridge Design Handbook Session* [Video]. Retrieved from http://media.aisc.org/NASCC2013/B3.mp4.

Kitipornchai, S. & Trahair, N. (1980). Buckling Properties of Monosymmetric I-Beams. *Journal of the Structural Division*, ASCE, *106*(STS), 941-957.

Lawson, R., & Nethercot, D. (1985). Lateral stability of I-beams restrained by profiled sheeting. *The Struct. Engr.*, London, 63B(1), 3-13.

Luttrell, L. D., & Steel Deck Institute. (2004). *Diaphragm design manual*. Canton, Ohio: Steel Deck Institute.

Nethercot, D., & Trahair, N. (1975). Design of diaphragm-braced I-beams. *J. Struct. Div.*, ASCE, 101(10), 2045–2061.

New York State Department of Transportation. (2009). *US Route 219: Southern Expressway*. Retrieved December 28, 2014 from https://www.dot.ny.gov/regional-offices/region5/projects/us-route-219-section5/photos

Owen, T. (2013, April 29). Composite floor system [Web log post]. Retrieved December 28, 2014, from http://tanya1.myblog.arts.ac.uk/2013/04/29/task-8-ludwig-mies-van-der-rohe-alumni-hall/

Texas Department of Transportation (2014). *Bridge Standards.* Retrieved December 28, 2014, from http://www.dot.state.tx.us/insdtdot/orgchart/cmd/cserve/standard/bridge-e.htm

Timoshenko, S., & Gere, J. M. (1961). *Theory of elastic stability*. New York: McGraw-Hill.

U.S. Department of Transportation Federal Highway Administration. (2013). *LRFD Steel Girder Super Structure Design Example.* Retrieved December 28, 2014, from http://www.fhwa.dot.gov/bridge/lrfd/us_ds3.cfm

Wang, L., & Helwig, T. A. (2005). Critical imperfections for beam bracing systems. *Journal of Structural Engineering*, *131*(6), 933-940.

Weeks, J. (2014, December 28). John James Audubon Bridge LA-10 Mississippi River crossing at New Roads [Web log post]. Retrieved December 28, 2014, from http://www.johnweeks.com/river_mississippi/pages/lmiss19.html

Winter, G., (1960) Lateral bracing of columns and beams. *Trans Am. Soc. Civ. Eng.*, 125, 809-825.

Ziemian, R. D. (2010). *Guide to stability design criteria for metal structures*. Hoboken, N.J: John Wiley & Sons.

APPENDIX A

DESIGN EXAMPLE

Beam Properties:

Stocky #2 girder

n, Number of beams = 4

t_d, Thickness of deck = 20 cm

s_g, Beam spacing = 3.25 m

L_b, Unbraced length = 18.30 m ($L_b/d = 20$)

A, Cross sectional area = 18432 mm^2

$S_{x\text{-}x}$ = 4431999 mm^3

Calculation of Design Loads:

Self weight of the steel I-Beam:

$$18432\,mm^2 \times 7.85 \times 10^{-5}\,\frac{N}{mm^3} = 1.45\,\frac{N}{mm} = 1.45\,\frac{kN}{m}$$

Concrete slab:

$$23.6\,\frac{kN}{m^3} \times 3.25\,m \times 0.20\,m = 15.34\,\frac{kN}{m}$$

Live load $\left(40\quad \frac{lb}{ft^2}\right) = \left(1.9052\quad \frac{kN}{m^2}\right)$

$$1.9052\,\frac{kN}{m^2} \times 3.25\,m = 6.19\,\frac{kN}{m}$$

Design load: $w = 1.45 + 15.34 + 6.19 = 22.98\quad \frac{kN}{m}$

Design moment: $M = \frac{w \times L_b^{\ 2}}{8} = 962\quad kNm$

Load Factor for the construction condition =1.3

Maximum bending stress: $\sigma = 1.3 \times \frac{M}{S_{x-x}} = 283\quad MPa$

Check beam buckling capacity:

According to the AISC (2010) limit state of lateral torsional buckling is can be checked according to the limiting laterally unbraced length, Lr which is defined below within the Equation B.1. Capacity of a beam alone can be checked with Equation 2.3 as well.

$$L_r = 1.95 * r_{ts} * \frac{E}{0.7F_y}\sqrt{\frac{Jc}{S_{x-x}h_0} + \sqrt{\left(\frac{Jc}{S_{x-x}h_0}\right)^2 + 6.76\left(\frac{0.7F_y}{E}\right)^2}} \quad \text{(B.1)}$$

where,

L_r = Limiting laterally unbraced length for the limit state of inelastic lateral-torsional buckling, mm

r_{ts} = Effective radius of gyration $= \frac{\sqrt{I_y C_w}}{S_x} = 72.89$ mm;

E = Modulus of elasticity of steel, 200 000 MPa;

F_y = Specified minimum yield stress, 345 MPa;

J = Torsional constant, 1489536 mm^4;

c = coefficient, 1 for doubly symmetric I-shapes;

S_x = Elastic section modulus taken about the x-axis, 4431999 mm^3;

h_0 = Distance between the flange centroids, 714 mm;

I_y = Moment of inertia about the principal axis, 65956224 mm^4;

C_w = Warping constant, 8406035382639 mm^6;

L_r is calculated as 7107 mm. $L_b > L_r$. Limit state of lateral-torsional buckling applies. Lateral torsional buckling capacity of a beam alone is not enough to carry a 210 MPa stress level due to bending.

Determine shear diaphragm parameters:

According to the Chapter 5, a diaphragm with four times the ideal stiffness need to be selected.

From Equation 2.1 M_{cr} is obtained as 283.32 kNm.

"m" factor is taken as 0.5 from Table 2. 1 for top flange loading case without an intermediate brace. C_b^* is 0.80. M_u for 210 MPa bending stress is 930.72 kNm.

From the data above, Q_{req}, Q_i is 1923.50 kn/rad. A total deck stiffness of 7694 kN/rad must be provided. Applying Equation 2.17(b)

$$s_d = \left(\frac{n-1}{n}\right) * s_g = \frac{3}{4} * 3.25 = 2.4375 \text{ m.}$$

$$G' = \frac{Q}{s_d} = ' \frac{7694}{2.4375} = 3156.51 \text{ kN/m/rad.}$$

A suitable diaphragm can be selected by using Luthrell (2004).